Contribution of CT and MRI in the analysis of fetal craniofacial malformations

Catherine Garel, Saskia Vande Perre, Lucie Guilbaud, Véronique Soupre, Eléonore Blondiaux, Hubert Ducou Le Pointe

Contribution of CT and MRI in the analysis of fetal craniofacial malformations

Catherine Garel [1], Saskia Vande Perre [1], Lucie Guilbaud [2], Véronique Soupre [3,4], Eléonore Blondiaux [1], Hubert Ducou le Pointe [1]

1. Service de Radiologie, Hôpital d'Enfants Armand-Trousseau APHP, Paris, France, Sorbonne Université
2. Service de Médecine Fœtale, Hôpital d'Enfants Armand-Trousseau APHP, Paris, France, Sorbonne Université
3. Service de Chirurgie Maxillo-faciale et Chirurgie Plastique, Hôpital Necker Enfants-Malades, APHP, 75015 Paris, France
4. Centre de référence Fentes et Malformations Faciales, APHP, 75015 Paris, France

Corresponding author:
Catherine Garel
Service de Radiologie, Hôpital d'Enfants Armand-Trousseau
26 Avenue du Dr Arnold Netter
75012 Paris, France
Tel: +33 1 71 73 82 08
Fax: +33 1 44 73 65 11
Email: catherine.garel@aphp.fr

Contribution of CT and MRI in the analysis of fetal craniofacial malformations

Abstract

A wide range of craniofacial malformations can be diagnosed in utero using ultrasonography. However, even in the best hands and conditions of examination, some anatomical structures cannot be properly analyzed by this technique. The aim of this pictorial essay is to show the additional value of fetal Magnetic Resonance Imaging and Computed Tomography in this setting and to illustrate the role of these modalities in various craniofacial malformations: craniosynostosis, facial clefts, ear, eye and nose abnormalities, otomandibular dysplasias and facial cephaloceles.

Keywords

Introduction

Craniofacial malformations may be isolated or part of a genetic syndrome. They encompass a variety of disorders including craniosynostosis, facial clefts, ear, eye and nose abnormalities, otomandibular dysplasias and facial cephaloceles. Craniofacial malformations are some of the most common birth defects [1] and occur in approximately 0.5-1 in 500 live births [2]. The prevalence of facial clefts and craniosynostosis is around 0.15% and 0.05% respectively [3].

Prenatal screening using 2D and 3D ultrasonography can accurately detect some craniofacial malformations. However, in many cases, a targeted scan focusing on the fetal face and searching for additional anomalies is required to improve US diagnostic accuracy. Even in the best hands and conditions of examination, some structures cannot be analyzed by US and the use of fetal Magnetic Resonance Imaging (MRI) and computed tomography may be very contributive.

The aim of this pictorial essay is to illustrate the contribution of fetal MRI and computed tomography in the analysis of some craniofacial malformations.

Craniosynostosis

Premature closure of one or several calvarial sutures results in significant cranial and/or facial changes in shape and morphology, which may be detected by ultrasonography. However, this diagnosis remains challenging and many isolated craniosynostoses are overlooked prenatally. Diagnostic accuracy is improved by the use of 3D ultrasound and computed tomography [4] (Fig 1). Syndromic craniosynostosis is less common with associated anomalies being present, involving particularly the brain, the hands and the feet. In this setting, fetal computed tomography and MRI (Fig 2) may be useful additional modalities [4-7].

Ear malformations

When isolated, ear malformations are very rarely diagnosed in utero because external ears are not evaluated at screening ultrasound and middle and inner ears cannot be properly analyzed using ultrasound. Ultrasound diagnostic accuracy is increased by the use of 3D that can demonstrate anomalies of size, position and shape of the external ears. These anomalies are commonly associated with middle ears malformations (Fig 3 and 4). The tympanic cavity and the ossicles can be depicted by fetal MRI [8,9] such that aural atresia may be diagnosed prenatally. Computed tomography may also demonstrate abnormal tympanic cavity but MRI should be favored as it is a non-ionizing modality. Conversely, if other facial malformations are observed and particularly if retrognathism is present, there is concern for otomandibular dysplasia and computed tomography may be very useful, as shown below. Inner ears anomalies are much less commonly associated with external ears anomalies except for some conditions such as CHARGE association (Fig 5). Inner ears are well depicted by fetal MRI and particularly semicircular canals and cochlea [10], making it possible to identify incomplete cochlear partition or vestibular hypoplasia with absent semicircular canals.

Eye malformations

Ocular malformations such as cataracts, microphtalmia, anophtalmia, hypo- and hypertelorism can be depicted by ultrasound [11]. Colobomas and colobomatous cysts may also be observed. However, ultrasound analysis depends on fetal position, amount of amniotic fluid and thickness of the maternal wall. Independently of these factors, fetal MRI allows better analysis of the orbital content (Fig 6) and the eye globe (Fig 7) [12,13]. However, it must be stressed that the diagnosis of cataract is based on ultrasonography, the abnormal lens content being unidentified by MRI. The size of the orbit is influenced by the size of the ocular globe and is better appreciated by computed tomography (Fig 8). However, prenatally, evaluation of the orbital size has no clinical impact. Dacryocystoceles result from imperforation of the membrane of Hasner between the nasolacrimal duct and the nasal cavity. They appear as uni- or bilateral anechoic lesions, medial to the eye globe and are typically observed in the third trimester [11]. They are usually depicted by ultrasonography and do not require further investigation by fetal MRI.

Nose malformations

The nasal cavity is well demonstrated by fetal MRI and arrhinia may be depicted [13]. Arrhinia may be unilateral in the setting of proboscis lateralis and is usually associated with microphtalmia, brain and cranial vault anomalies and less commonly, midline clefting [14]. Such a malformation is very rare and associated anomalies could be more easily analyzed by fetal MRI.   Binder phenotype is characterized by vertical nasal bone, flattened nasal bridge and maxillary hypoplasia. These features are identified by ultrasonography (Fig 9) and are a hallmark of chondrodysplasia punctata. This group of skeletal dysplasias is characterized by multiple punctate cartilaginous stippling, mainly in the epiphyses and is caused by various etiologies [15]. In our experience, the most common type encountered in the prenatal period is the brachytelephalangic one. It may be associated with stenosis of the spinal canal with possible subsequent spinal cord compression [16]. Computed tomography (Fig 9) and fetal MRI can demonstrate such a stenosis. Moreover, in this type of chondrodysplasia punctata, poor mineralization of the cervical spine may result in cervical kyphosis. It can be suggested at ultrasonography but is better demonstrated by fetal MRI [15] or computed tomography (Fig 10).

Orofacial clefts

Cleft lip and/or palate are the most common congenital craniofacial anomaly [17]. Cleft may be uni- or bilateral and can affect the lip, the alveolar ridge (Fig 11) and the hard and soft palates. Cleft lip with or without cleft palate is more common than isolated cleft palate and is less likely to be part of a syndrome [18]. Cleft lip is easy to detect using ultrasound and does not require complementary MRI as a diagnostic tool. Cleft alveolus may be subtle and more difficult to detect using ultrasound. At MRI, the alveolar process is best displayed on axial slices [19] (Fig 11). Isolated cleft palate without cleft lip is a challenging ultrasound diagnosis and MRI is a useful adjunct to ultrasound. T2-weighted coronal and sagittal views provide information on the secondary palate. In cleft palate, abnormal communication is visible between the mouth and the naso-pharynx and appears as a T2 bright signal intensity (related to amniotic fluid) extending upwards from the tongue [17,19] (Fig 12). Cleft palate may be observed in the setting of Robin sequence, in association with mandibular retrognathism and glossoptosis. Posterosuperior displacement of the tongue is usually better depicted on MRI than on ultrasound [20] (Fig 12). When cleft lip and/or palate is identified in utero, thorough search for possible associated malformations is required. Some cerebral anomalies may be overlooked by ultrasound and identified by MRI only [21] (Fig 13). In the setting of orofacial cleft, there is no indication for fetal computed tomography.

Otomandibular dysplasias

Otomandibular dysplasias are characterized by the association of ears and mandible anomalies. They may be bilateral and symmetrical with predominant zygomatic and malar hypoplasia, in keeping with Treacher-Collins or Franceschetti syndrome, also named mandibulofacial dysostosis. Acrofacial dysostosis (Nager and Miller syndromes) is suggested when anomalies of the extremities are observed. In the oculoauriculovertebral spectrum, the anomalies are unilateral or bilateral and asymmetrical. Brain, cardiac, renal, intestinal and skeletal abnormalities are commonly associated [22]. Prenatal diagnosis of otomandibular dysplasia is challenging. Increased amniotic fluid volume is frequent and usually results from impaired swallowing secondary to micrognathia or orofacial clefting. Low-set ears, malformed ears, preauricular tags and micrognathism may be depicted by ultrasound [23]. Fetal MRI may be very contributive by demonstrating middle ear anomalies [8] and also possible associated brain malformations. Prenatal computed tomography can show skeletal anomalies and can evaluate the temporomandibular joints (Fig 14) with subsequent limitation of the mouth aperture and risk of nutritional and respiratory disorders at birth.

Facial cephaloceles

Most cephaloceles are occipital in location, frontal cephaloceles being observed in about 15% of cases. The majority of them show nasal protrusion while few demonstrate infraorbital or nasoethmoidal protrusion. In most cases, the diagnosis of cephalocele is achieved by ultrasonography and is based on identification of the bony defect and protruded brain tissue [24]. However, in frontal cephaloceles and particularly in frontoethmoidal location, the diagnosis may be more challenging with other entities such as dermoid cyst or glioma being discussed. Postnatally, computed tomography is used to evaluate the osseous defect and MRI helps visualize the content of the soft-tissue mass and search for a connection with the subarachnoid space [25]. Similarly in the prenatal period, MRI may be very helpful as evaluation of the nasoethmoidal area with ultrasound is usually difficult and hampered by the bony structures (Fig 15).

Conclusion

Craniofacial malformations are common and involve an anatomic area, which is difficult to analyze properly using prenatal ultrasonography even in the best conditions of sonographer's skill, maternal habitus and fetal presentation. The ultrasonographic examination of this area is hampered by the presence of many bony structures and poor contrast resolution of this imaging modality, such that many malformations cannot be analyzed precisely or are completely missed. This pictorial essay shows that the adjunct of fetal MRI may dramatically increase diagnostic accuracy of fetal craniofacial malformations. Less commonly, some malformations may also benefit from further analysis by prenatal computed tomography.

Conflict of interest: none

References

1. Yoon AJ, BN Pham ,KM Dipple (2016) Genetic Screening in Patients with Craniofacial Malformations. J Pediatr Genet 5: 220-224
2. Byvaltsev V, O Belykh ,E Belykh (2012) New aspects in the epidemiology of craniofacial anomalies. World Neurosurg 77: 599-600
3. Mak ASL ,KY Leung (2019) Prenatal ultrasonography of craniofacial abnormalities. Ultrasonography 38: 13-24
4. Helfer TM, AB Peixoto, G Tonni et al (2016) Craniosynostosis: prenatal diagnosis by 2D/3D ultrasound, magnetic resonance imaging and computed tomography. Med Ultrason 18: 378-385
5. Rubio EI, A Blask ,DI Bulas (2016) Ultrasound and MR imaging findings in prenatal diagnosis of craniosynostosis syndromes. Pediatr Radiol 46: 709-718
6. Saliba S, B Morel, M Gonzales et al (2018) Variable prenatal presentation of Pfeiffer syndrome: Suggested aids to prenatal sonographic diagnosis. Prenat Diagn 38: 349-356
7. Werner H, P Castro, P Daltro et al (2018) Prenatal diagnosis of Apert syndrome using ultrasound, magnetic resonance imaging, and three-dimensional virtual/physical models: three case series and literature review. Childs Nerv Syst 34: 1563-1571
8. Katorza E, C Nahama-Allouche, V Castaigne et al (2011) Prenatal evaluation of the middle ear and diagnosis of middle ear hypoplasia using MRI. Pediatr Radiol 41: 652-657
9. Moreira NC, J Teixeira, R Raininko et al (2011) The ear in fetal MRI: what can we really see? Neuroradiology 53: 1001-1008
10. Tilea B, C Garel, F Menez et al (2006) Contribution of fetal MRI to the diagnosis of inner ear abnormalities: report of two cases. Pediatr Radiol 36: 149-154
11. Ondeck CL, D Pretorius, J McCaulley et al (2018) Ultrasonographic prenatal imaging of fetal ocular and orbital abnormalities. Surv Ophthalmol 63: 745-753
12. Bremond-Gignac D, H Copin, M Elmaleh et al (2010) [Fetal ocular anomalies: the advantages of prenatal magnetic resonance imaging]. J Fr Ophtalmol 33: 350-354
13. Nagarajan M, KG Sharbidre, SH Bhabad et al (2018) MR Imaging of the Fetal Face: Comprehensive Review. Radiographics 38: 962-980
14. Galie M, LC Clauser, R Tieghi et al (2019) The arrhinias: Proboscis lateralis literature review and surgical update. J Craniomaxillofac Surg 47: 1410-1413
15. Blask AR, EI Rubio, KA Chapman et al (2018) Severe nasomaxillary hypoplasia (Binder phenotype) on prenatal US/MRI: an important marker for the prenatal diagnosis of chondrodysplasia punctata. Pediatr Radiol 48: 979-991
16. Garnier A, S Dauger, D Eurin et al (2007) Brachytelephalangic chondrodysplasia punctata with severe spinal cord compression: report of four new cases. Eur J Pediatr 166: 327-331
17. Zheng W, B Li, Y Zou et al (2019) The prenatal diagnosis and classification of cleft palate: the role and value of magnetic resonance imaging. Eur Radiol 29: 5600-5606

18. Abramson ZR, ZS Peacock, HL Cohen et al (2015) Radiology of Cleft Lip and Palate: Imaging for the Prenatal Period and throughout Life. Radiographics 35: 2053-2063

19. Tian M, L Xiao, N Jian et al (2019) Accurate diagnosis of fetal cleft lip/palate by typical signs of magnetic resonance imaging. Prenat Diagn 39: 883-889

20. Resnick CM, TD Kooiman, CE Calabrese et al (2018) An algorithm for predicting Robin sequence from fetal MRI. Prenat Diagn 38: 357-364

21. de Milly MN, M Alison, O Arthurs et al (2013) Is fetal cerebral MRI worthwhile in antenatally diagnosed isolated cleft lip with or without palate? Prenat Diagn 33: 273-278

22. Burglen L, V Soupre, PA Diner et al (2001) [Oto-mandibular dysplasias: genetics and nomenclature of syndromes]. Ann Chir Plast Esthet 46: 400-409

23. Castori M, F Brancati, R Rinaldi et al (2006) Antenatal presentation of the oculo-auriculo-vertebral spectrum (OAVS). Am J Med Genet A 140: 1573-1579

24. Weichert J, F Hoellen, M Krapp et al (2017) Fetal cephaloceles: prenatal diagnosis and course of pregnancy in 65 consecutive cases. Arch Gynecol Obstet 296: 455-463

25. Van Wyhe RD, ES Chamata ,LH Hollier (2016) Midline Craniofacial Masses in Children. Semin Plast Surg 30: 176-180

Figures

Fig 1: isolated sagittal craniosynostosis

Fig 1a and 1b depict a scaphocephaly in a fetus of 27 weeks of gestation. Ultrasound biometry (Fig 1a) shows a small biparietal diameter (4th centile) while the head circumference is markedly increased (92nd centile). Occipital bossing is well visible on this ultrasound midsagittal view (Fig 1b). At 30 weeks of gestation, 3D reformat computed tomography shows partial premature closure of the sagittal suture (arrow) just behind the anterior fontanelle (Fig1c).

Fig 2: syndromic right coronal craniosynostosis

At ultrasound, hypertelorism is visible on an axial view (Fig 2a) in this fetus of 33 weeks of gestation. The midline sagittal view (Fig 2b) shows turricephaly. At MRI (midsagittal T2 weighted-sequence) performed a week later, the corpus callosum is too short and thin (Fig 2c). On the same day, 3D reformat computed tomography (Fig 2d) shows superolateral elevation of right orbit (arrow) resulting from unilateral right coronal craniosynostosis (arrowhead). The latter is well depicted on the 2D reformat axial slice (Fig 2e).

Fig 3: bilateral aural atresia in a fetus with a cat-eye syndrome (retrognathia, imperforate anus and unilateral renal multicystic dysplasia were also identified by ultrasonography)

At ultrasound (Fig 3a), both external ears (arrow) are low-set, small and dysplastic. Axial (Fig 3b) and coronal (Fig 3c) T2-weighted sequences performed at 31 weeks of gestation show hypertelorism and bilateral absence of external auditory canal and tympanic cavity. The same slices (Fig 3d and e) acquired in a gestational age-matched control show the external auditory canals (open arrow) and the tympanic cavities (arrowhead).

Fig 4: isolated unilateral aural atresia in a fetus of 30 weeks of gestation (ultrasonography demonstrated deformity, small size and abnormal low position of the right external ear)

On the T2-weighted axial slice (Fig 4a), the right external auditory canal and the right tympanic cavity are absent. Computed tomography (Fig4b), performed on the same day, show normal inner ears and absence of ossicles on the right side, while ossicles are visible (arrow) on the left side.

Fig 5: abnormal internal ears in CHARGE syndrome (30 weeks of gestation)

On T2-weighted axial slices (Fig 5a and b), the petrous bones are small and the semicircular canals are not visible while the same slice performed in a gestational aged-matched control (Fig 5c) shows the posterior semicircular canals (arrows). The T2-weighted coronal slice shows in the control (Fig 5e) the superior (thick arrow) and the lateral (dotted arrow) semicircular canals, which are absent in the fetus with CHARGE syndrome (Fig 5d).

Fig 6: bilateral microphtalmia with colobomatous cyst

In this fetus of 26 weeks of gestation, ultrasound (Fig 6a) demonstrates a small eyeball (arrow) with a cyst (arrowhead) located in the inferonasal quadrant of the orbit. At 32 weeks of gestation, bilateral microphtalmia with colobomatous cyst (arrowheads) is well depicted by T2- weighted axial (Fig 6b) and coronal (Fig 6c) slices. The same findings are observed at 2.5 months of age on this T2-weighted coronal slice (Fig 6d).

Fig 7: left coloboma in a fetus with CHARGE syndrome (same fetus as Fig 5)

On this T2-weighted axial slice, coloboma appears as a focal defect with bulging of the posterior globe (arrow).

Fig 8: abnormal size of the eyeball

In this fetus of 27 weeks of gestation, ultrasound axial view (Fig 8a) shows small right eyeball (microphtalmia) and enlarged left eyeball (buphthalmos). The axial length is 10 mm and 16 mm on the right and left side respectively (normal axial length at this gestational age is around 12 mm). Computed tomography reformation in the coronal plane (Fig 8b) shows in the same fetus a small right orbit and an enlarged left one.

Fig 9: brachytelephalangic type of chondrodysplasia punctata at 23 weeks of gestation in a female fetus whose mother suffers from connectivitis. Spinal canal stenosis.

The ultrasound midline sagittal view (Fig 9a) of the fetus' face and brain shows a Binder phenotype with vertical nasal bone and flattened nasal ridge. The ultrasound midsagittal view of the lower part of the spine (Fig 9b) depicts stenosis of the spinal canal at the thoracolumbar junction (arrowheads). This stenosis is confirmed by computed tomography reformation in the midsagittal plane (Fig 9c, arrowheads). Computed tomography also shows bilateral tarsal stippling (arrows) and stippling of one femoral head (dotted arrow) (Fig 9d).

Fig 10: brachytelephalangic type of chondrodysplasia punctata in a male fetus at 26 weeks +4 of gestation.

In the midline sagittal plane, computed tomography reformation of the face (Fig 10a) and cervical spine (Fig 10b) demonstrates vertical nasal bone (arrow) and absent spina nasalis (arrowhead) in keeping with Binder phenotype. Spina nasalis is a small spur, which is normally observed at the base

of the columella. Poor mineralization and hypoplasia of the cervical vertebral bodies are well demonstrated (Fig 10b), which is confirmed on this midline T2 gradient echo slice of the spine, acquired at 5 days of age (Fig 10c).

Fig 11: cleft lip and alveolus in two fetuses of 32 (Fig 11 a and b) and 33 weeks (Fig 11 c and d) of gestation respectively.

Ultrasound (Fig 11 a and c) and MRI (Fig 11 b and d) axial views focused on the alveolar ridge. In the first fetus (Fig 11 a and b), the alveolar cleft (arrowhead) is unilateral and rather subtle (with a small gap) accounting for this type of cleft being often overlooked by ultrasonography. The cleft is better depicted by MRI (Fig 11b). In the second fetus, the cleft is bilateral with a protrusive premaxillary segment (arrow) and is well demonstrated by both imaging modalities.

Fig 12: cleft palate. T2-weighted midline sagittal slices.

In the first fetus (Fig 12a) of 32 weeks of gestation, the unilateral cleft lip and alveolus (not shown) is not associated with a cleft palate. The secondary palate appears as a hypointense linear structure (arrowhead) separating oral and nasal cavities. In the second fetus (Fig 12b) of 33 weeks of gestation, the bilateral cleft lip and alveolus (not shown) is associated with a cleft palate resulting in abnormal communication between the oral and nasal cavities and absence of visibility of the secondary palate. In the third fetus (Fig 12c) of 38 weeks of gestation, there is no cleft lip and alveolus but a cleft palate with posterosuperior displacement of the tongue and retrognathism in the setting of a Robin sequence.

Fig 13: labioalveolar clefts with associated anomalies in two fetuses of 32 weeks of gestation

In the first fetus, the T1 midline sagittal slice (Fig 13a) shows small anterior pituitary gland (arrow) with normal bright signal intensity and ectopic neurohypophysis (arrowhead) with normal bright signal intensity. In the second fetus, the T2-weighted coronal slice (Fig 13b) shows hypoplasia of both olfactory bulb (dotted arrow) and sulcus (open arrow) on the left side and absence of these structures on the right side.

Fig 14: oculo-auriculo-vertebral spectrum in a fetus of 29 weeks of gestation. Ultrasonography showed bilateral preauricular tags, mild retrognathism and polyhydramnios.

On 3D reformat computed tomography (Fig 14a), the left mandible (arrow) is mildly shorter than the right one. Left L1 hemivertebra is well demonstrated on the multiplanar reformat mode in the coronal view (Fig 14b). The sagittal view of the left mandible (Fig 14c, multiplanar reformat mode) shows underdevelopment of the ramus. This is confirmed by the 3D reformat computed tomography (Fig 14d) performed following termination three weeks later. The left temporomandibular joint is absent. The same findings, although less pronounced, were also observed on the right side (not shown).

Fig 15: frontoethmoidal cephalocele

This patient was referred for unilateral right ventriculomegaly at 28 weeks of gestation. Ultrasound examination (Fig 15a) revealed a defect (arrowhead) in keeping with enlarged fonticulus frontalis and a subcutaneous mass (arrow) adjacent to this defect. On the same day, at fetal MRI, the T2-weighted

midline sagittal slice (Fig 15b) showed an anterior cranial-base defect (arrowhead) in keeping with enlarged foramen caecum and a cephalocele (dotted arrow) extending into the defect. On the T2-weighted coronal slice (Fig 15c), the frontoethmoidal cephalocele is well visible (dotted arrow) with complete absence of the pericerebral fluid below the frontal lobe, unlike what is observed on the left side. After birth, at 8 days of age, the ethmoidal bony defect (arrowhead) is well visible on the 3D reformat computed tomography of the face (Fig 15d).

Fœtus A

U/S SA 27s2j SA(DDG) 27s2j			
BIP	63.5mm (*CFEF2) 25s1j	4%tile	
CC	264.7mm (*CFEF2) 29s2j	92%tile	

Figure7

PDF version
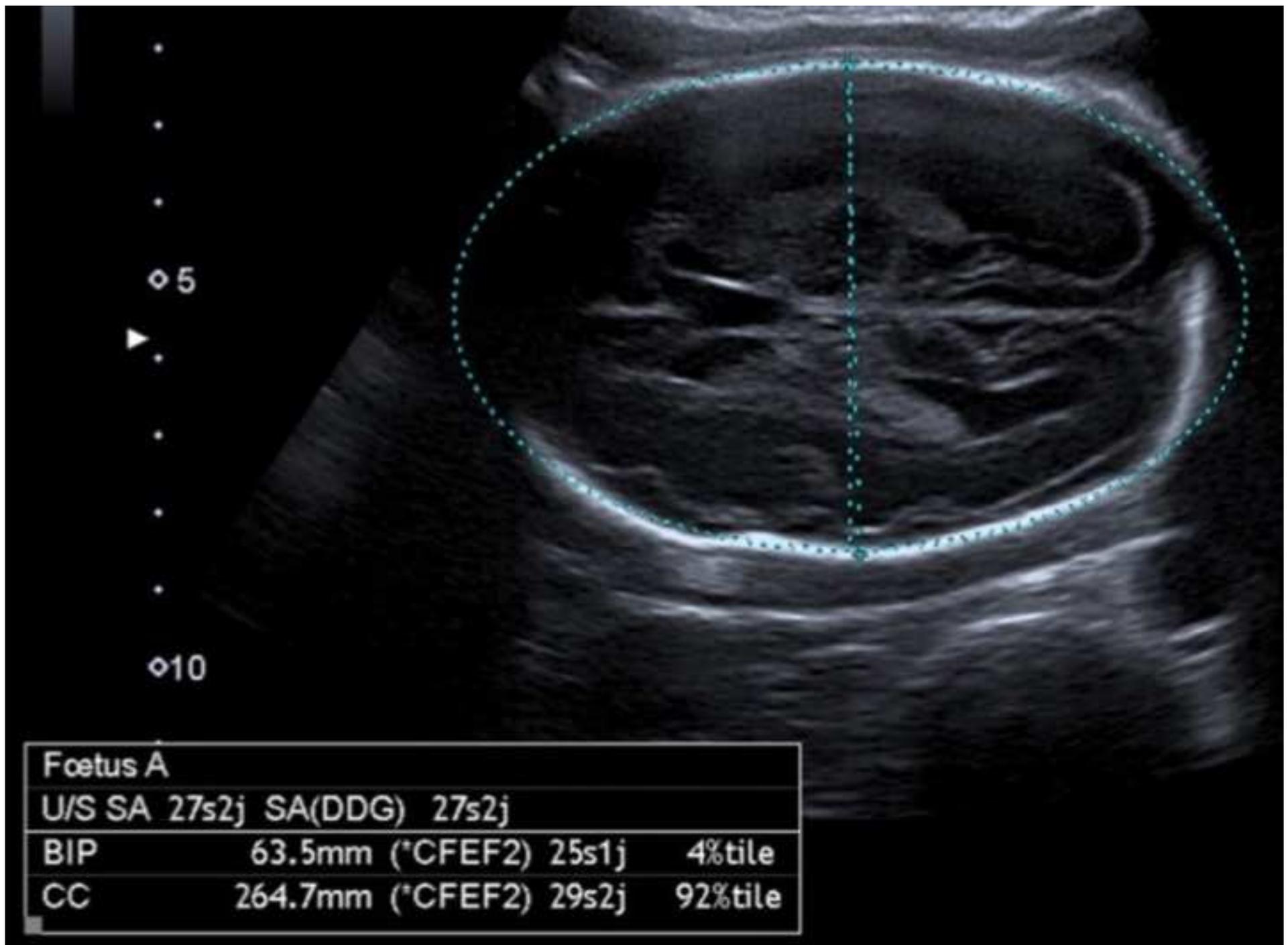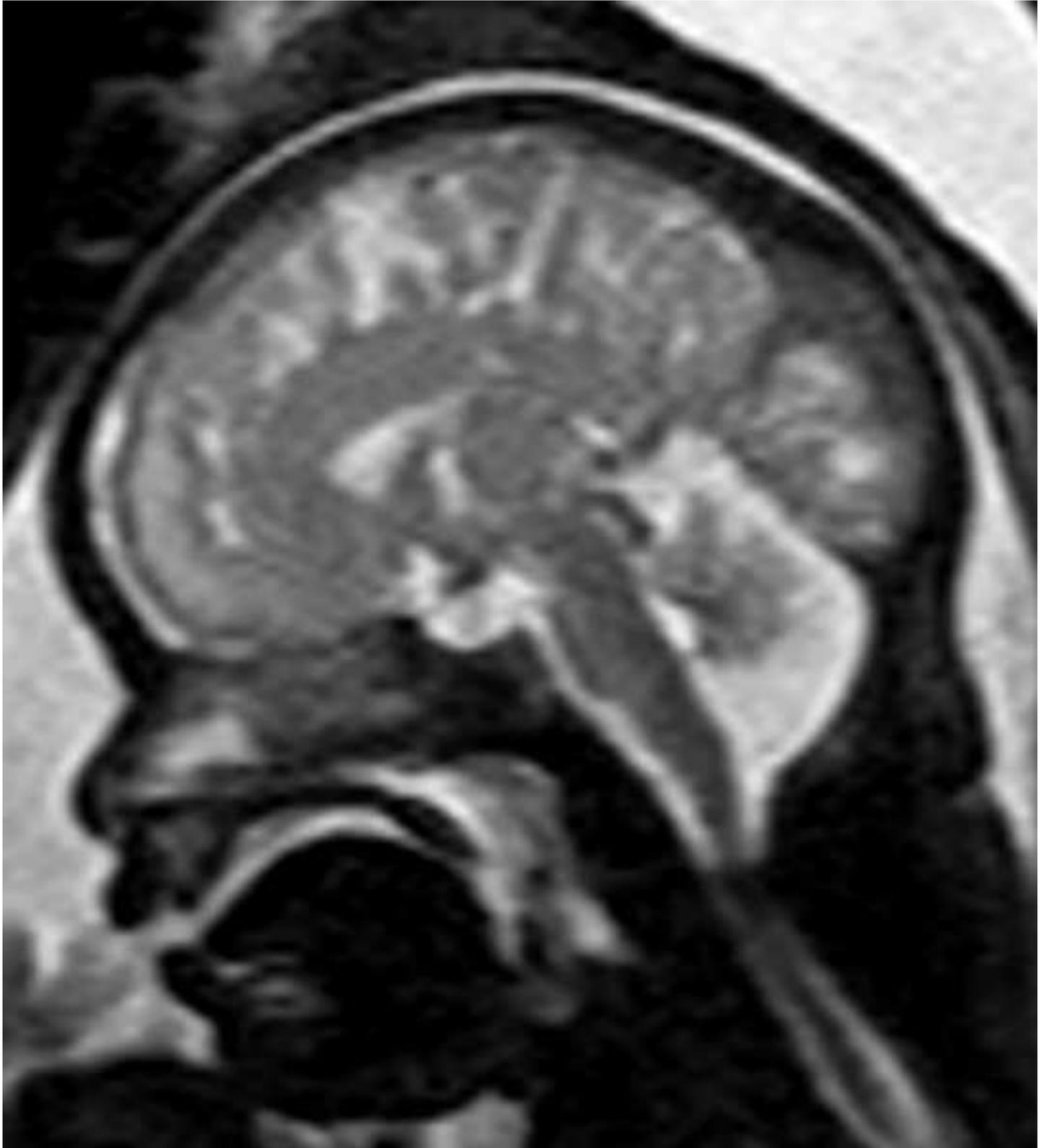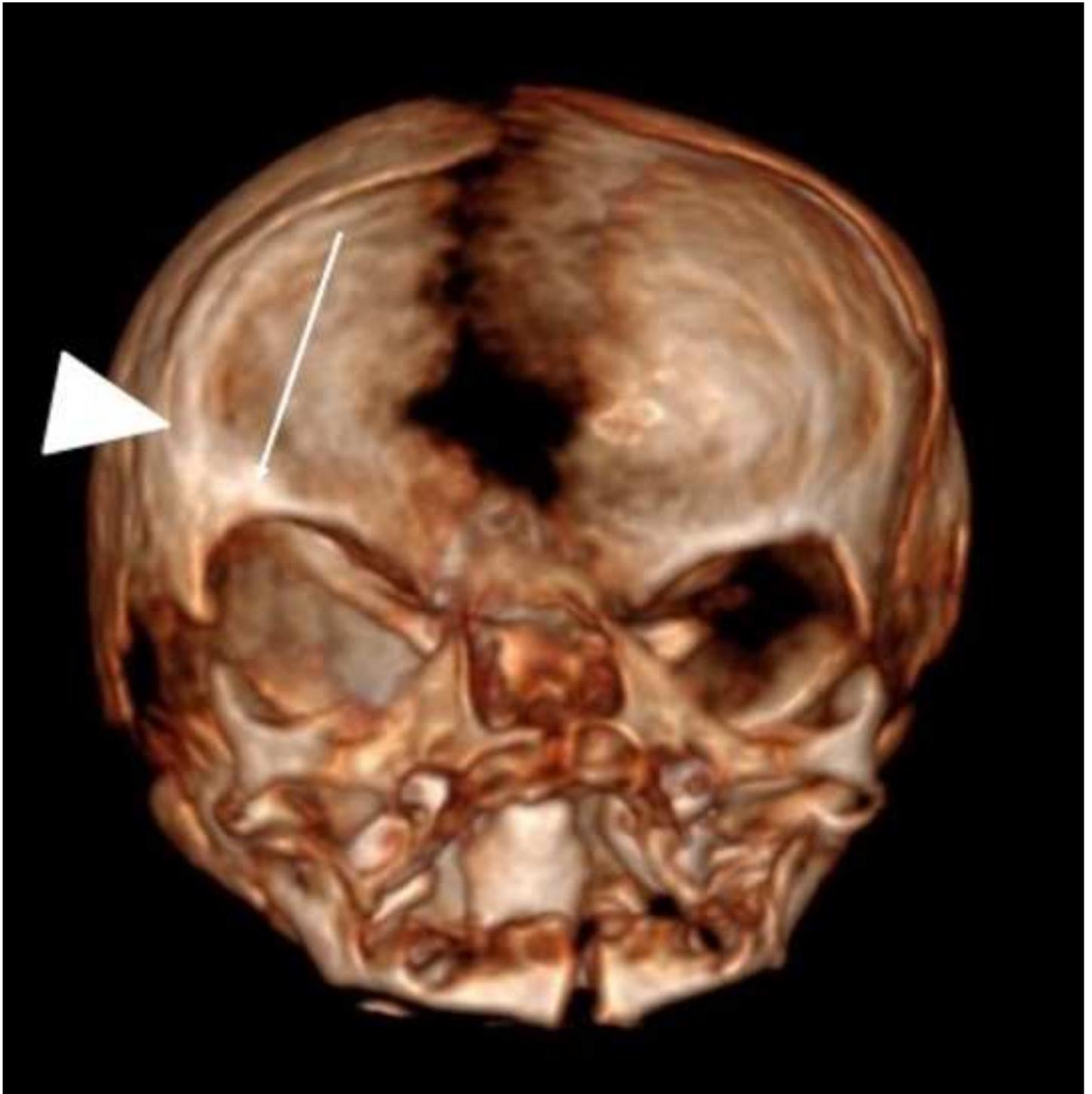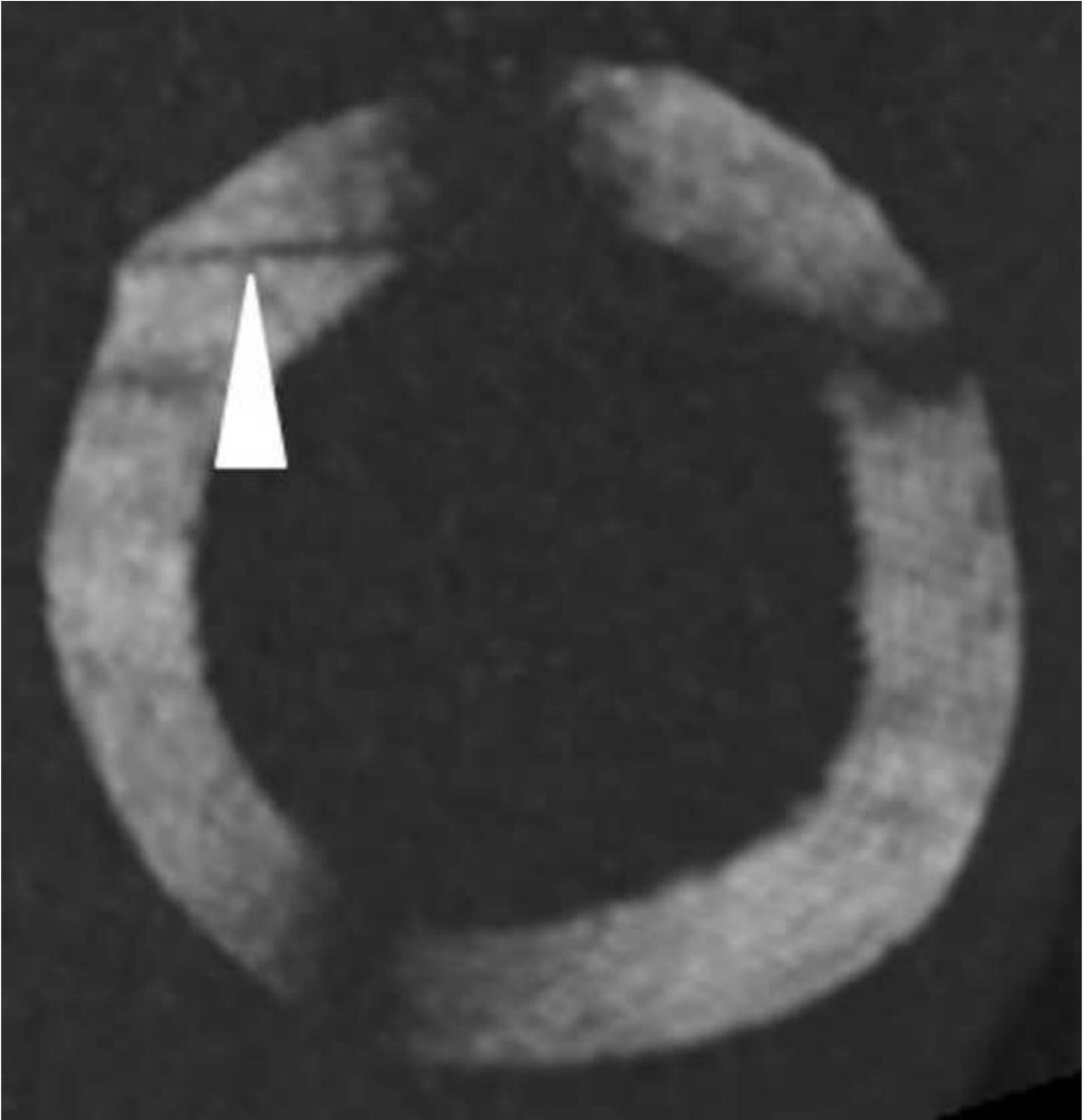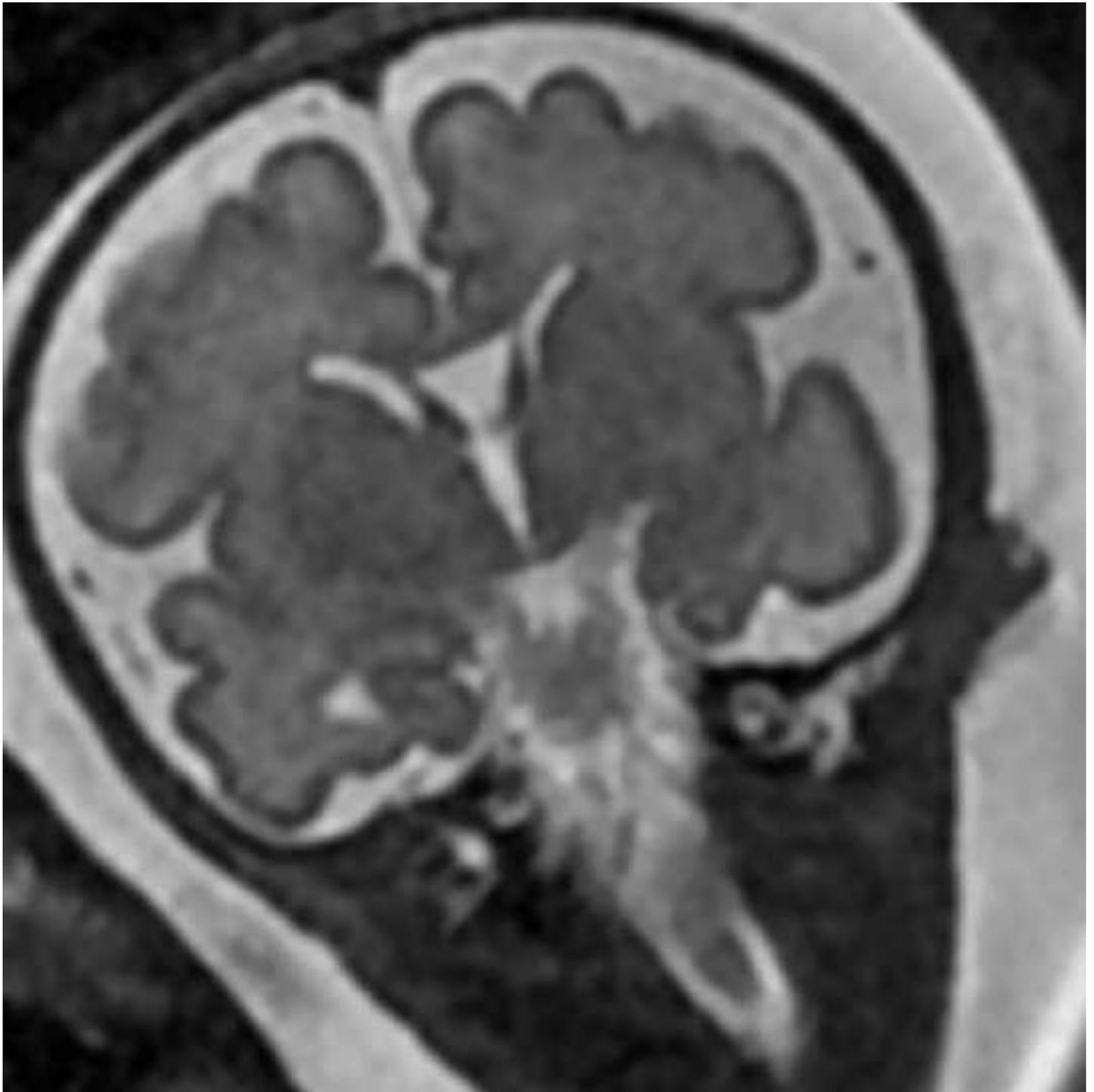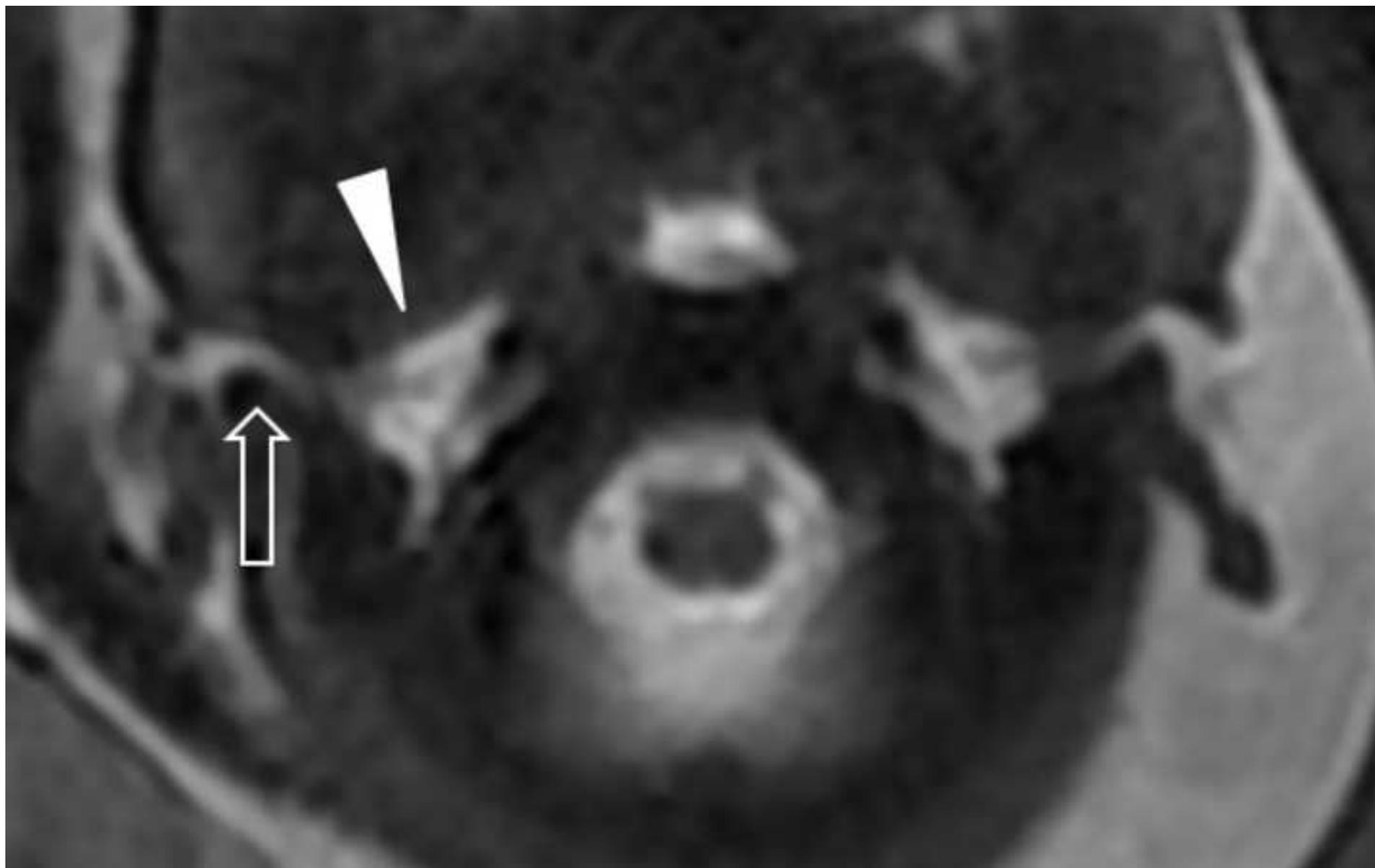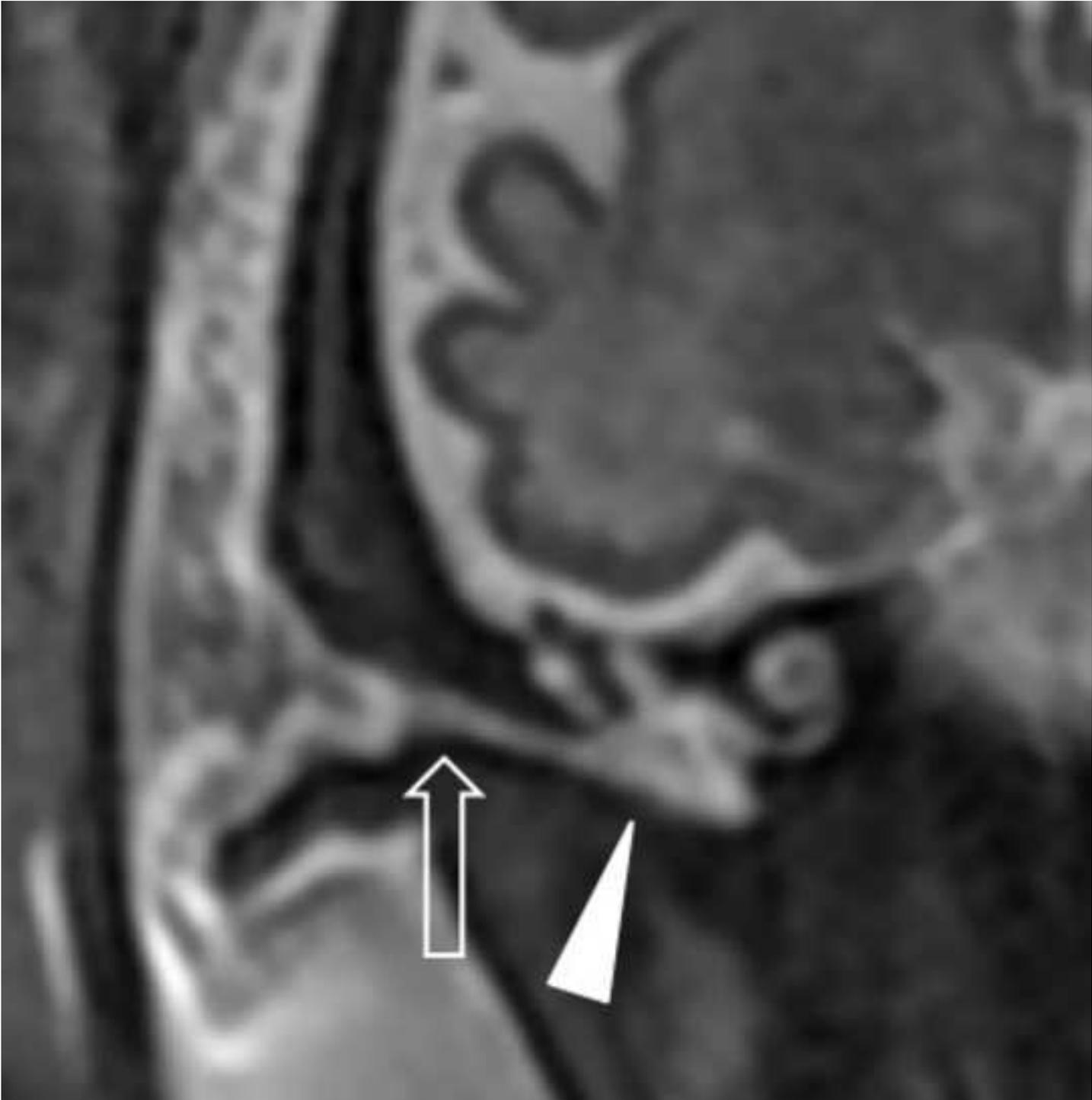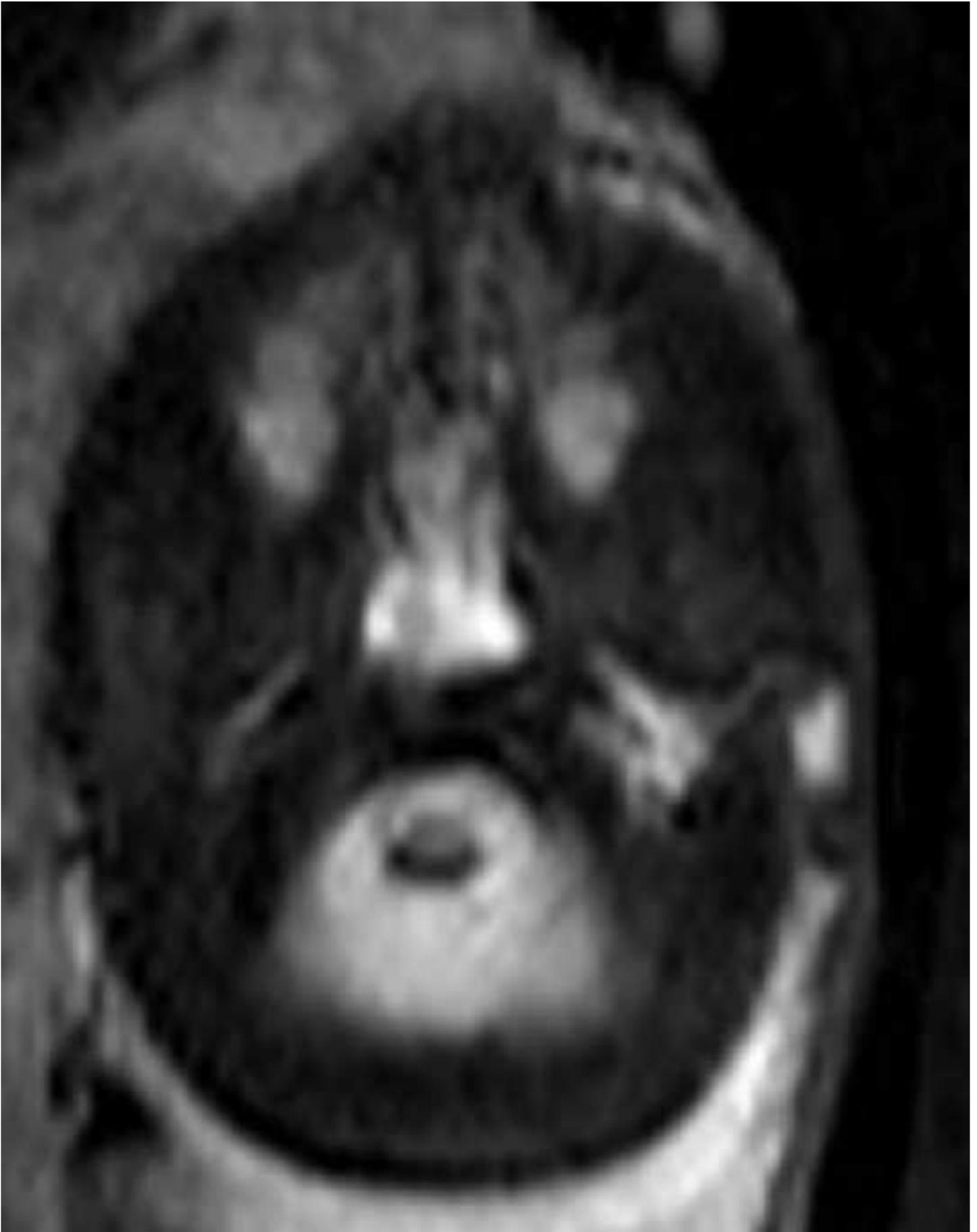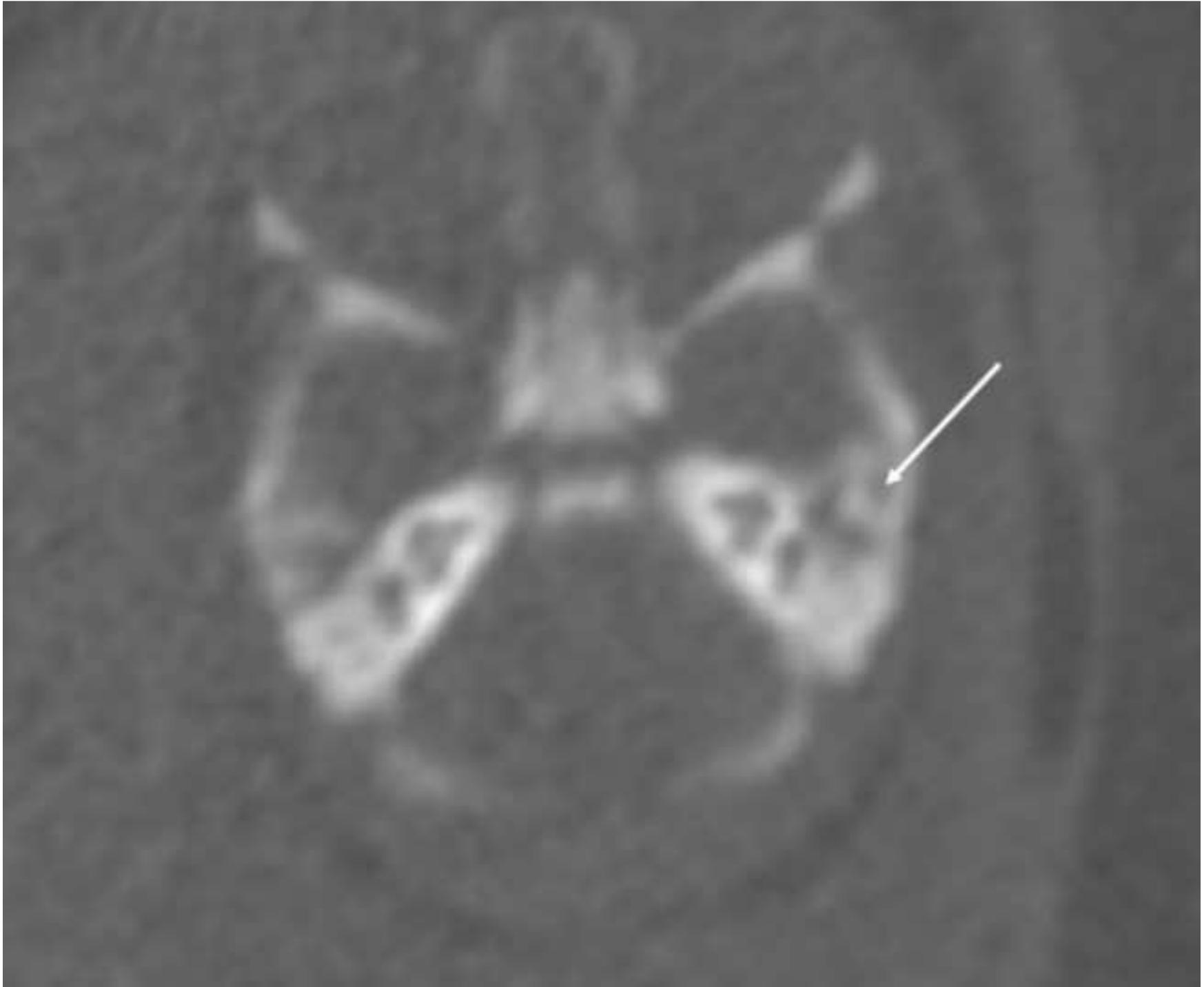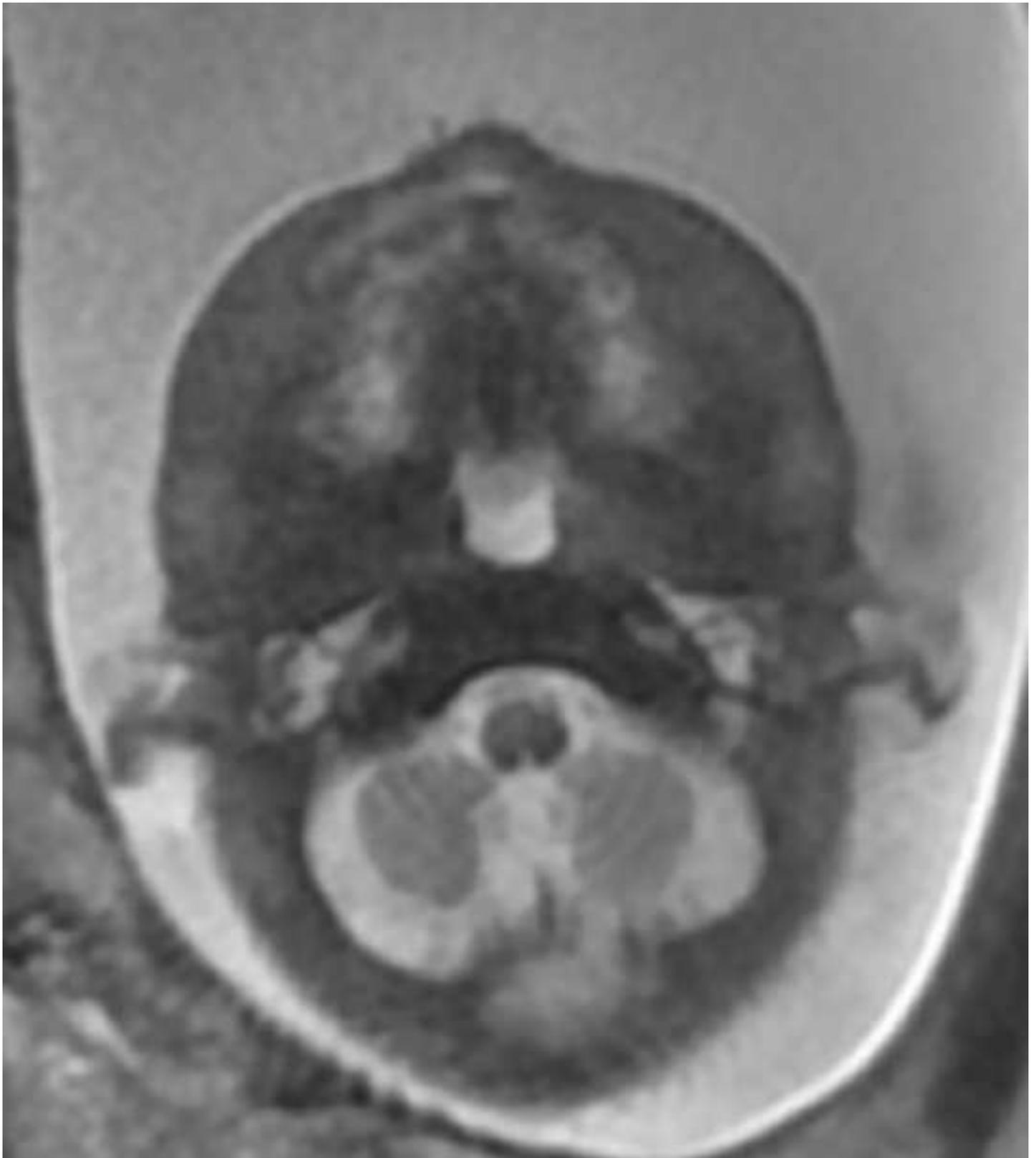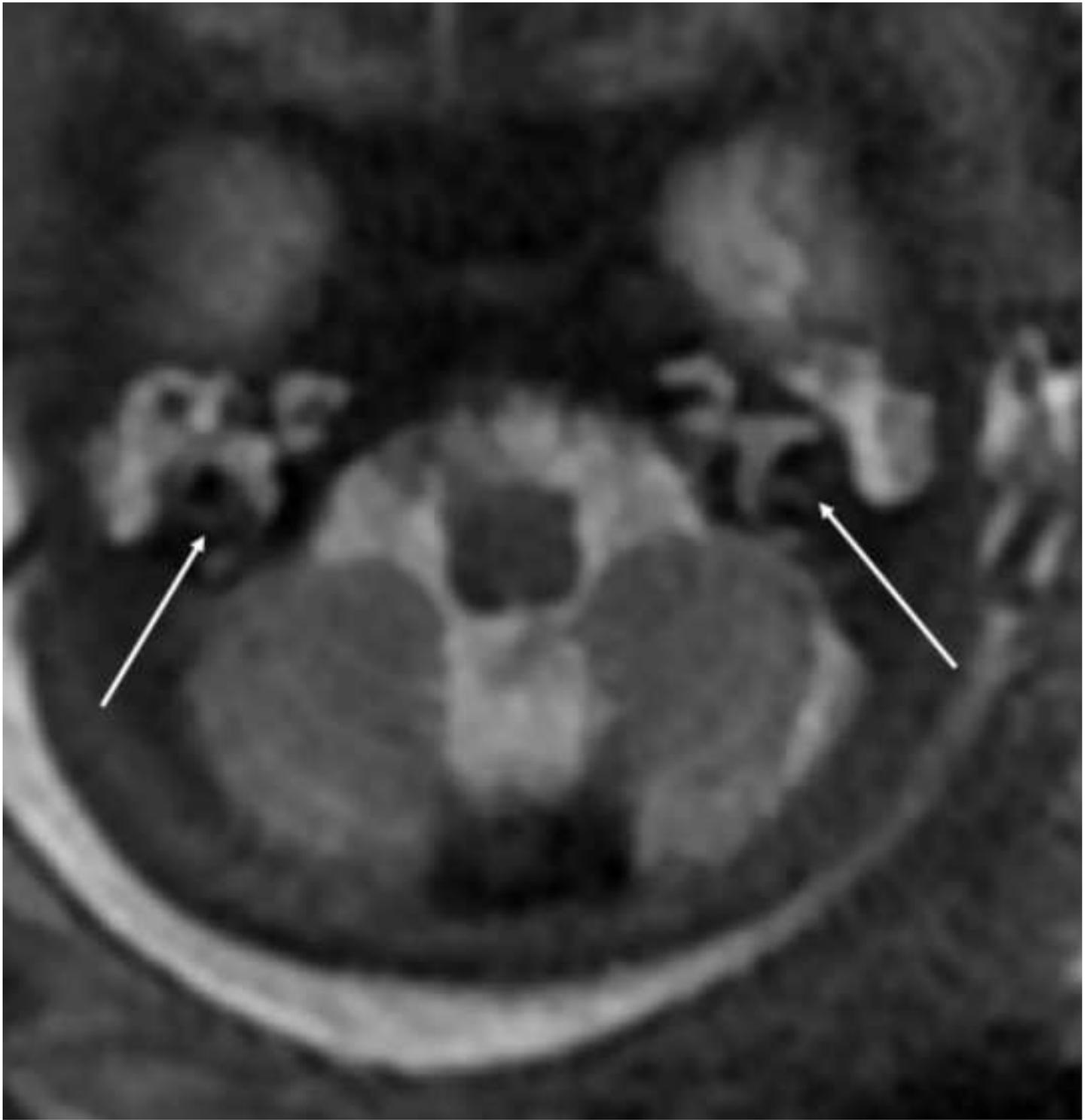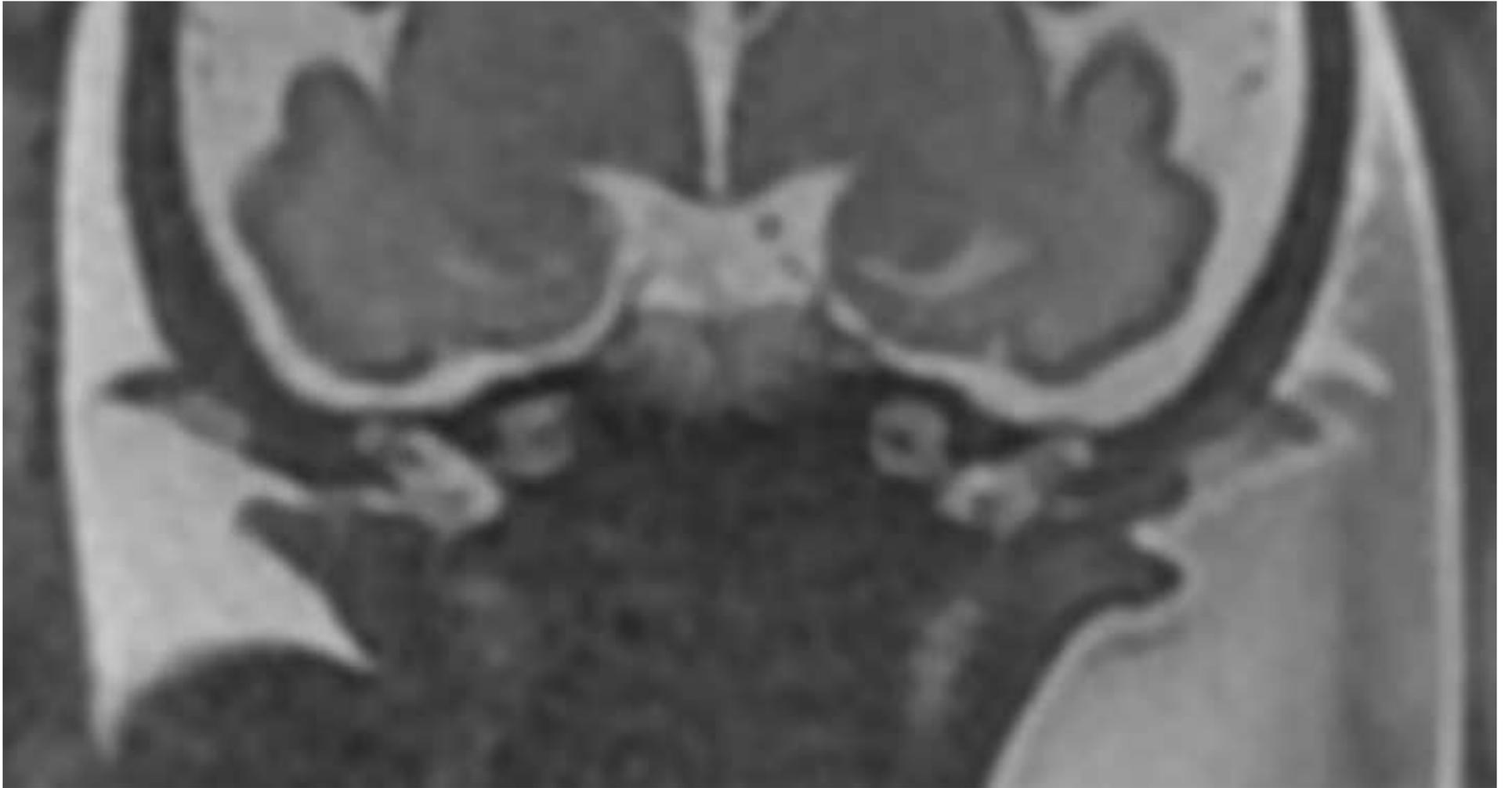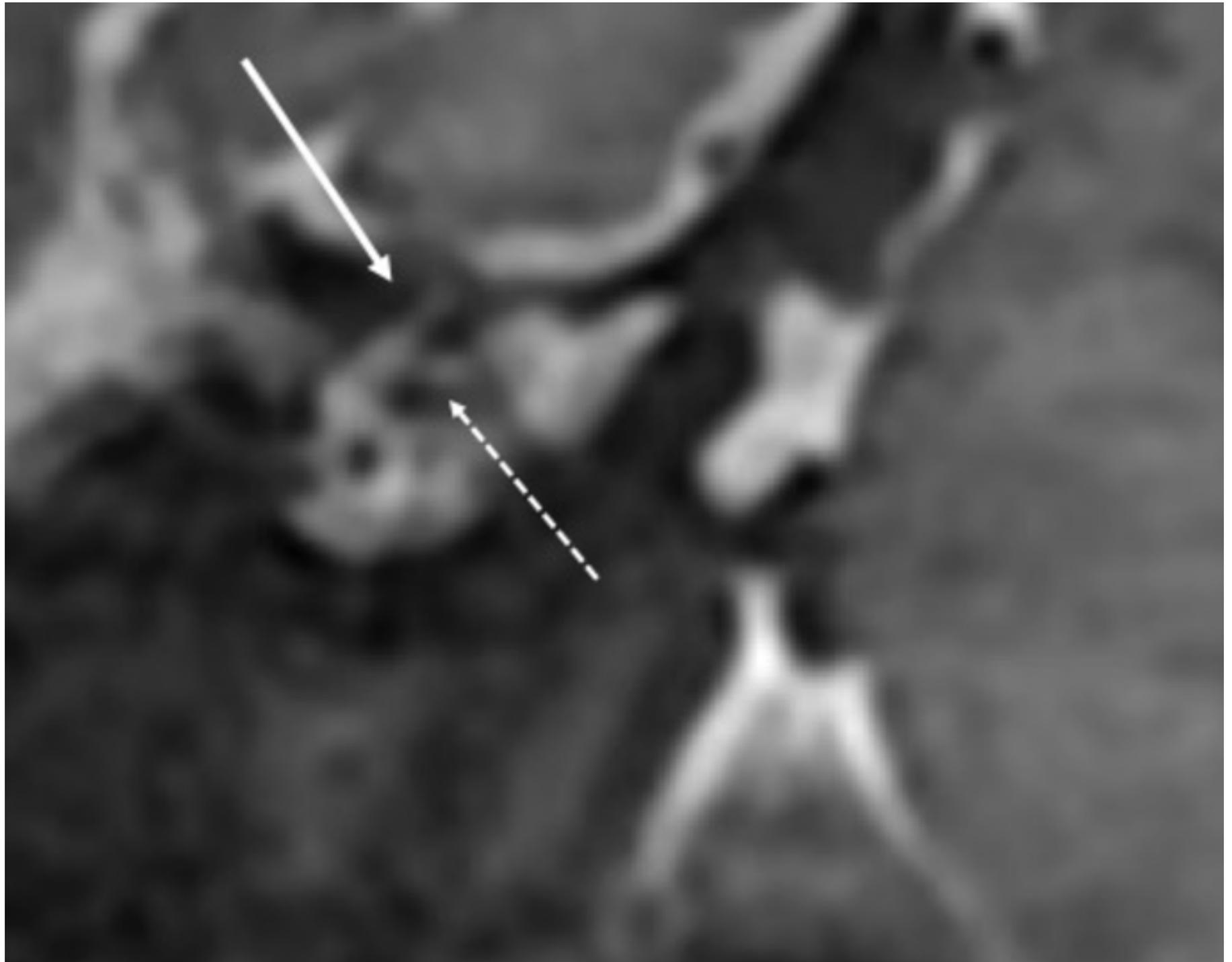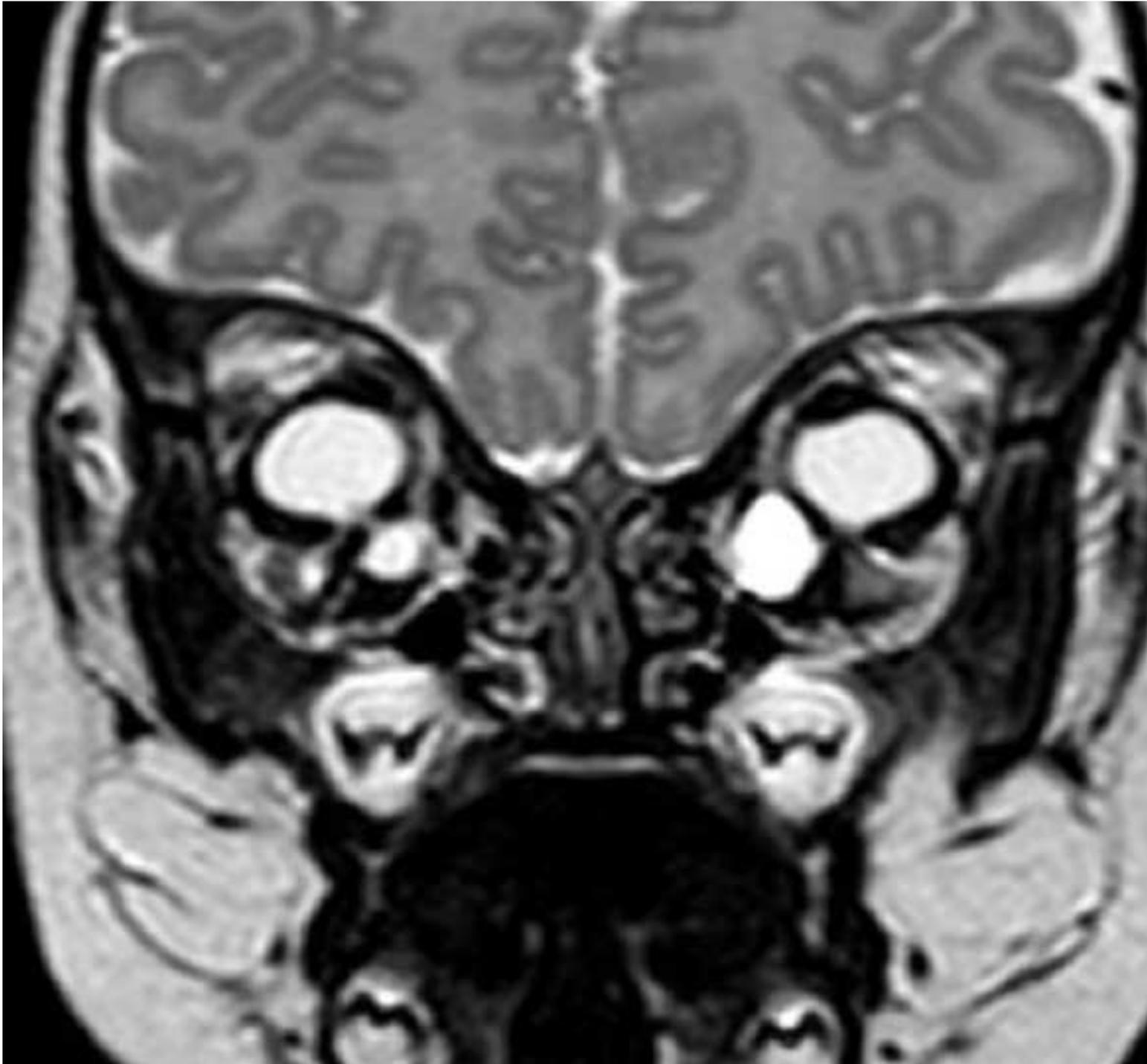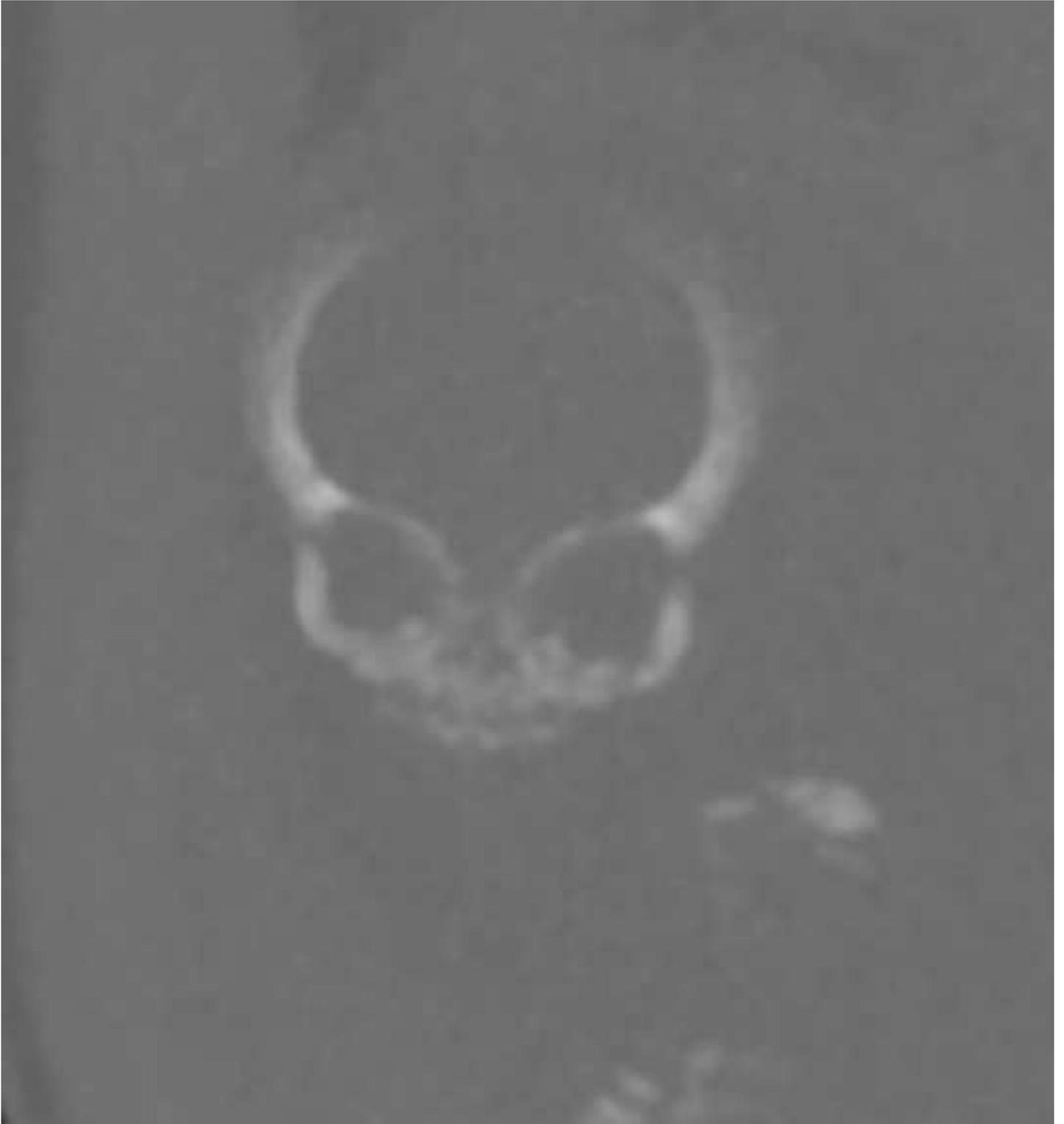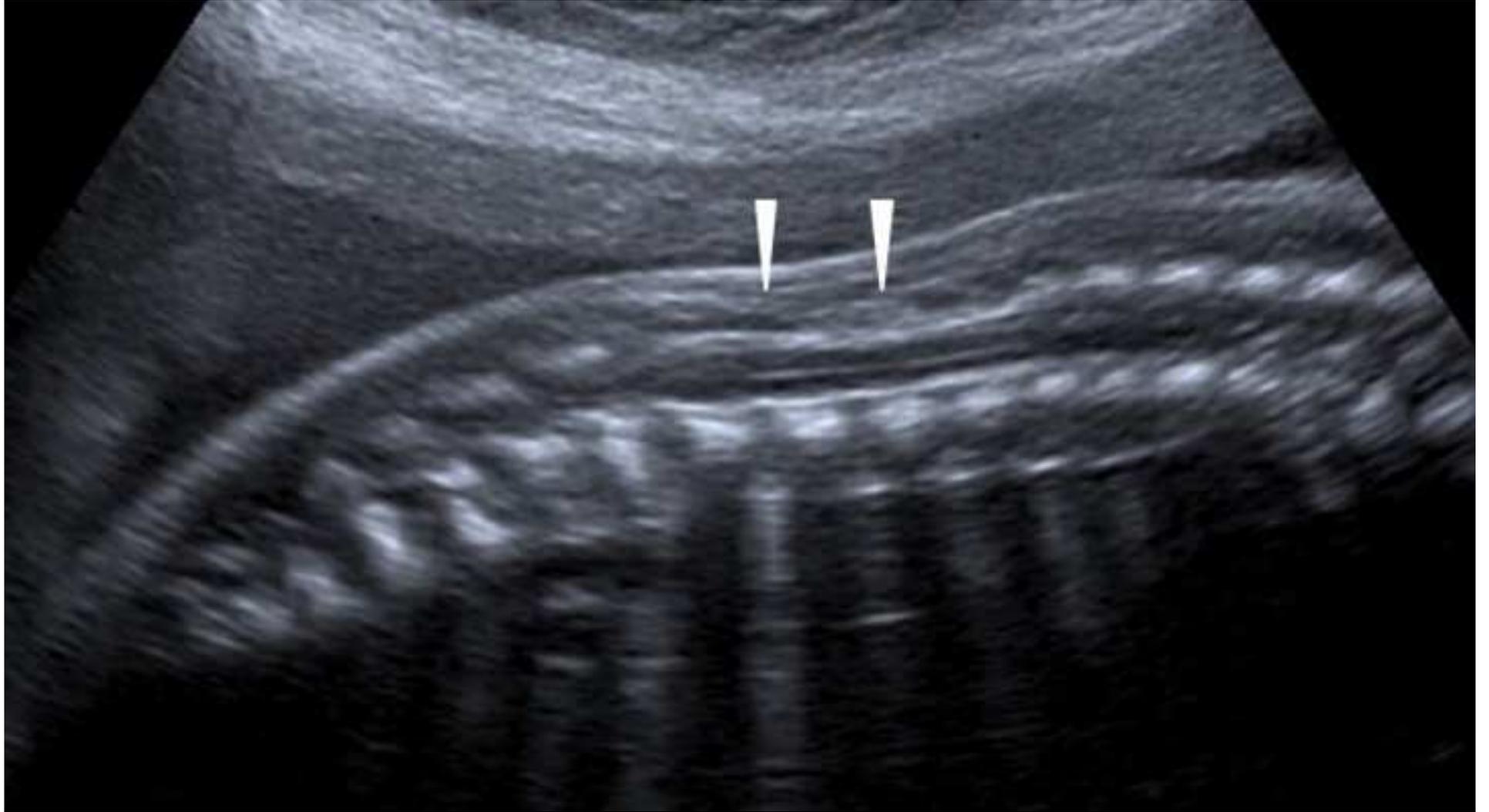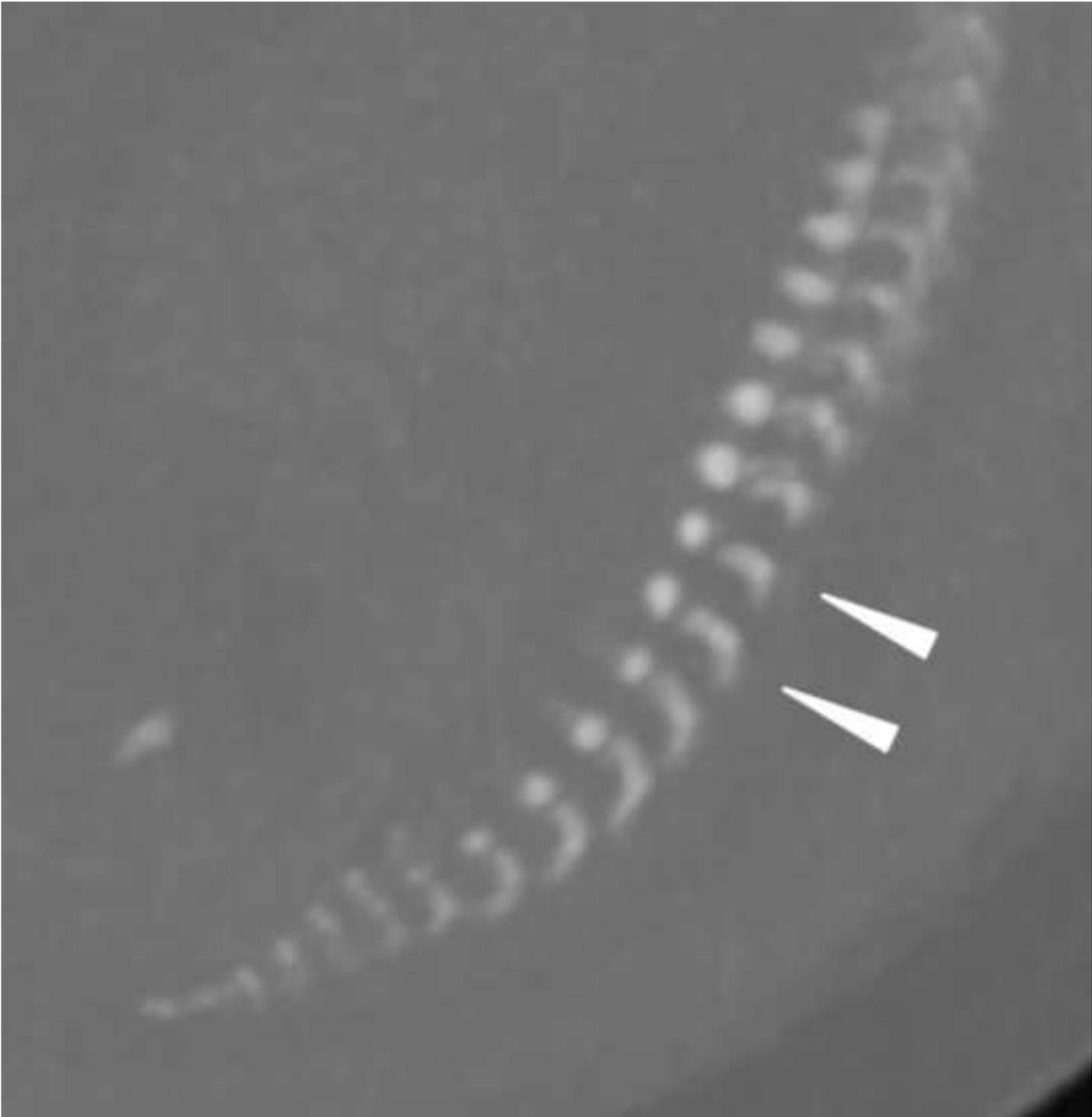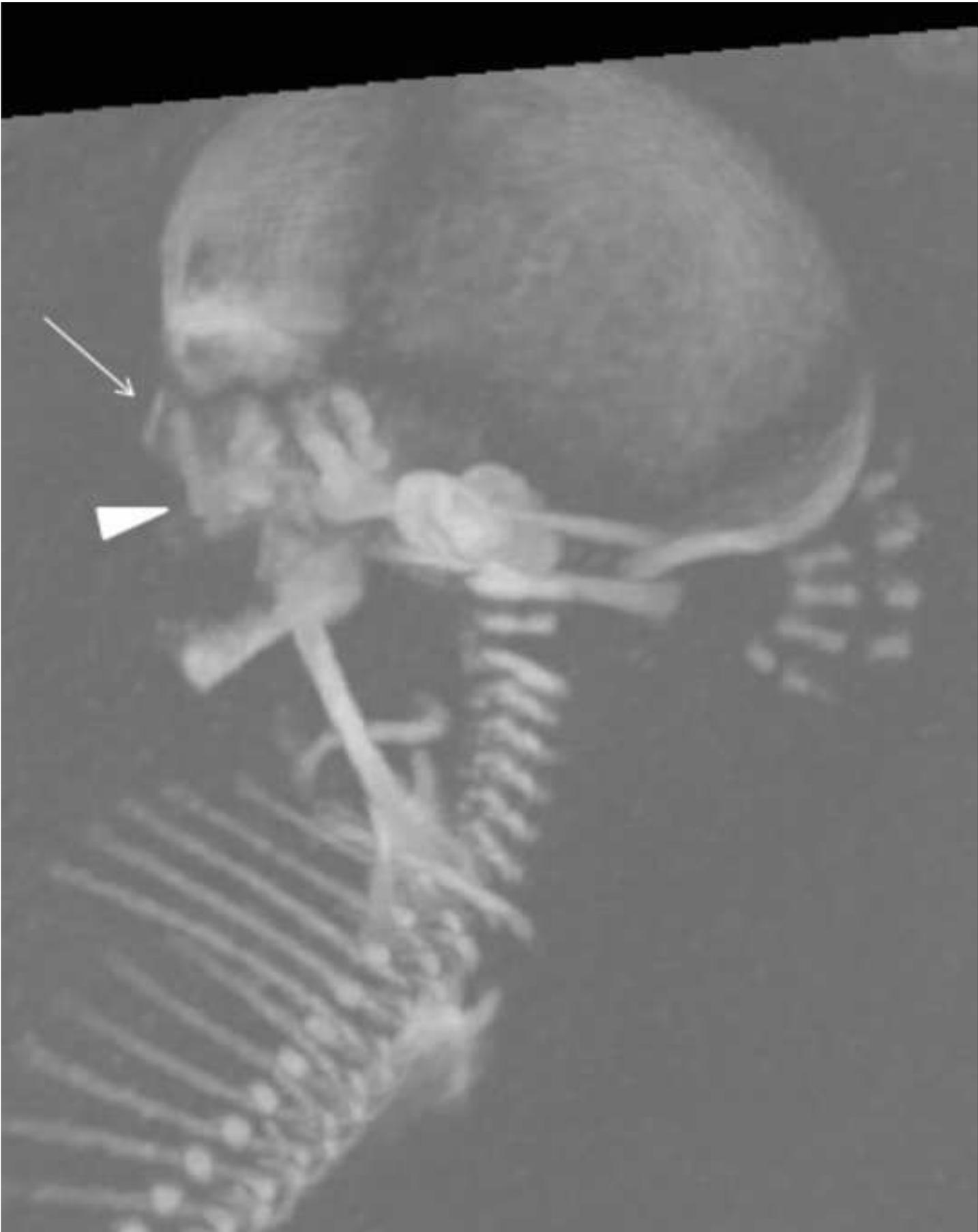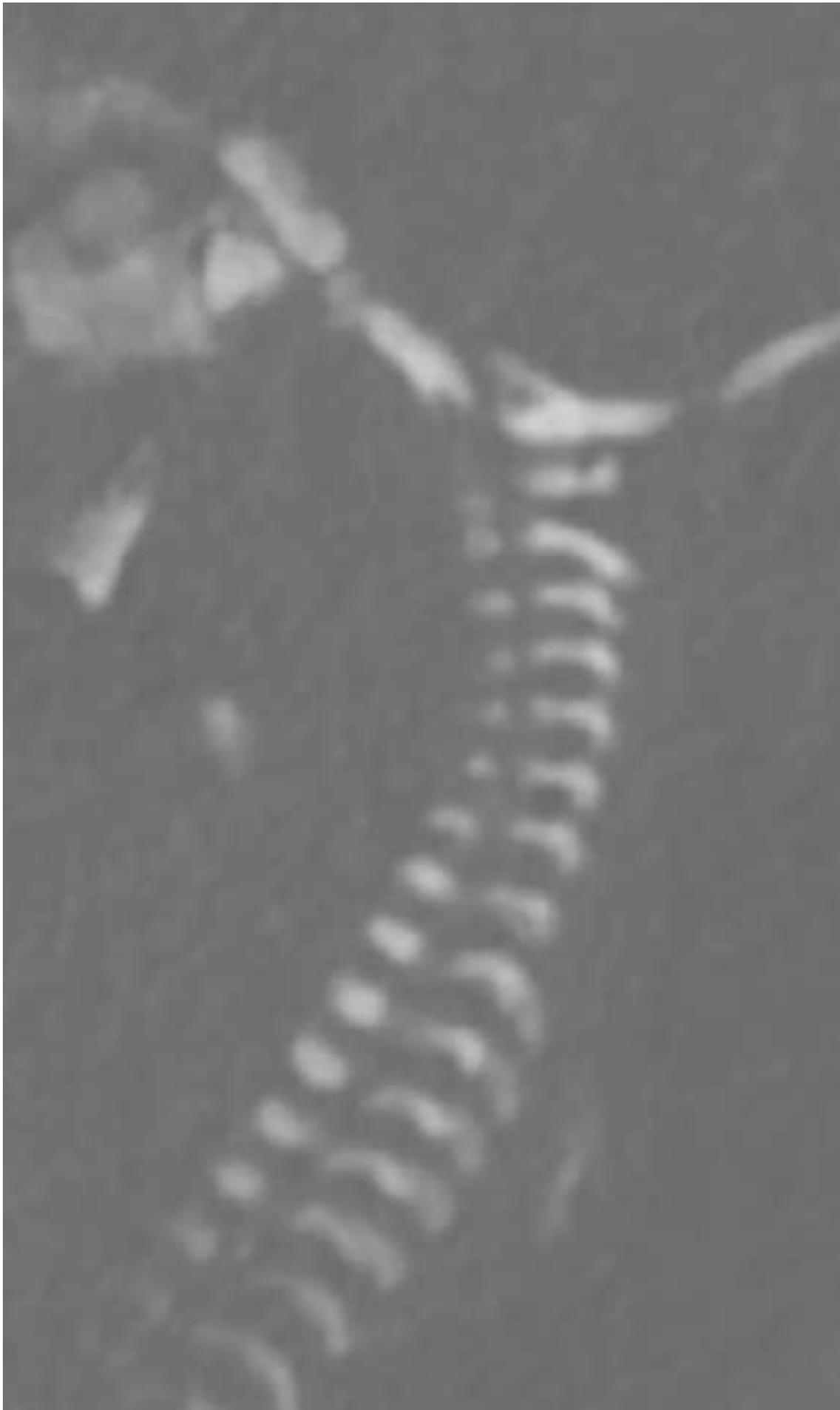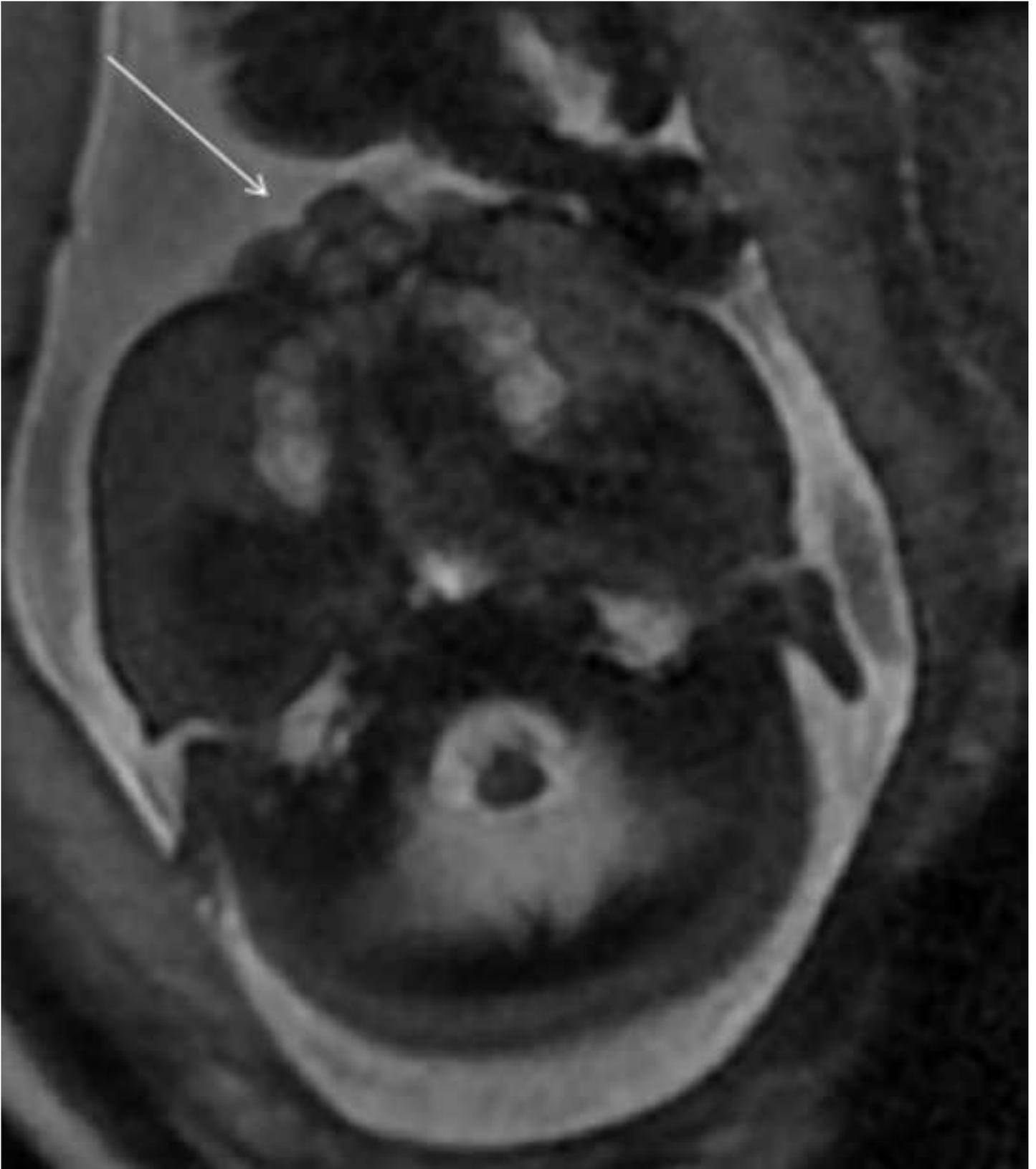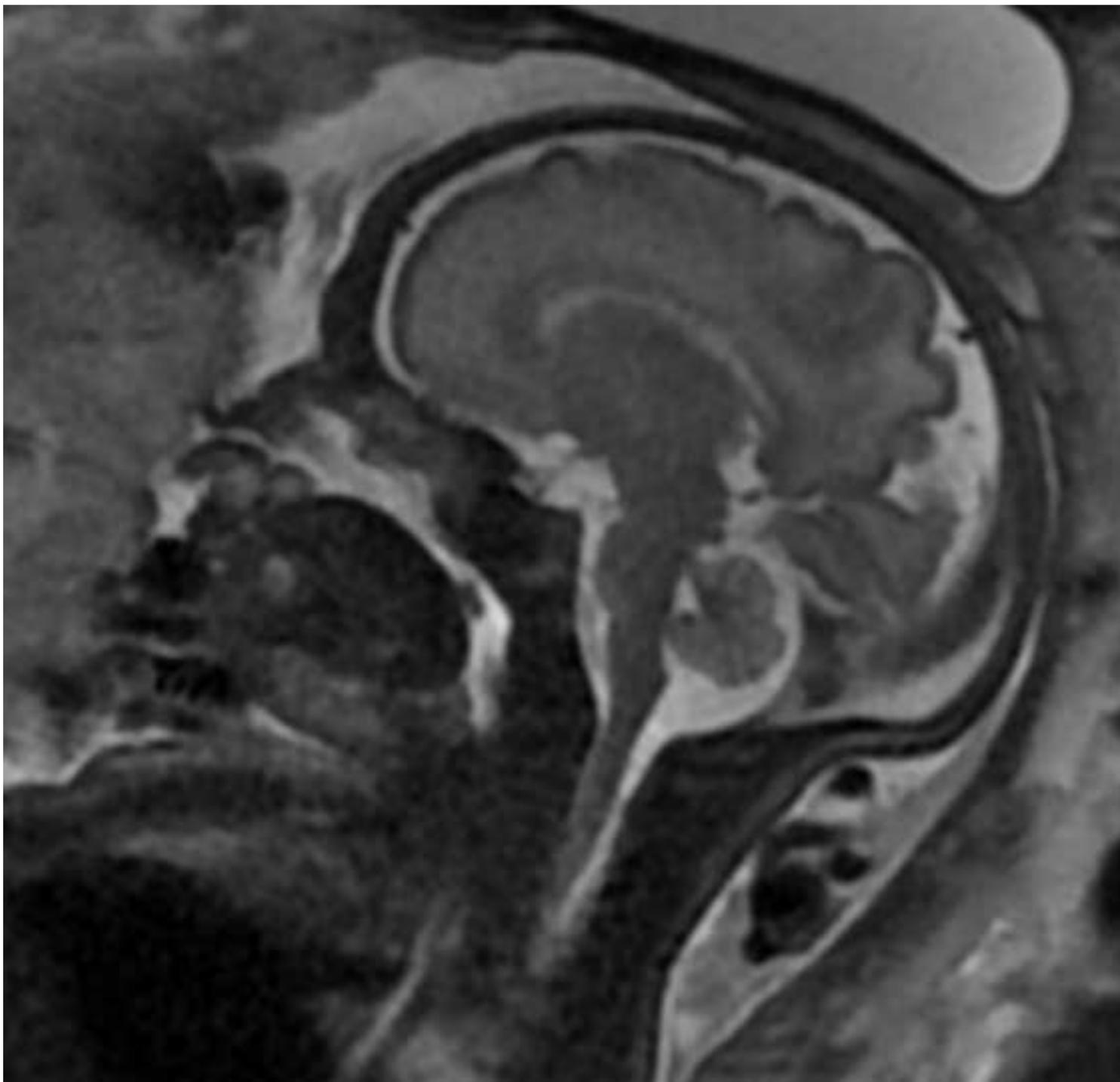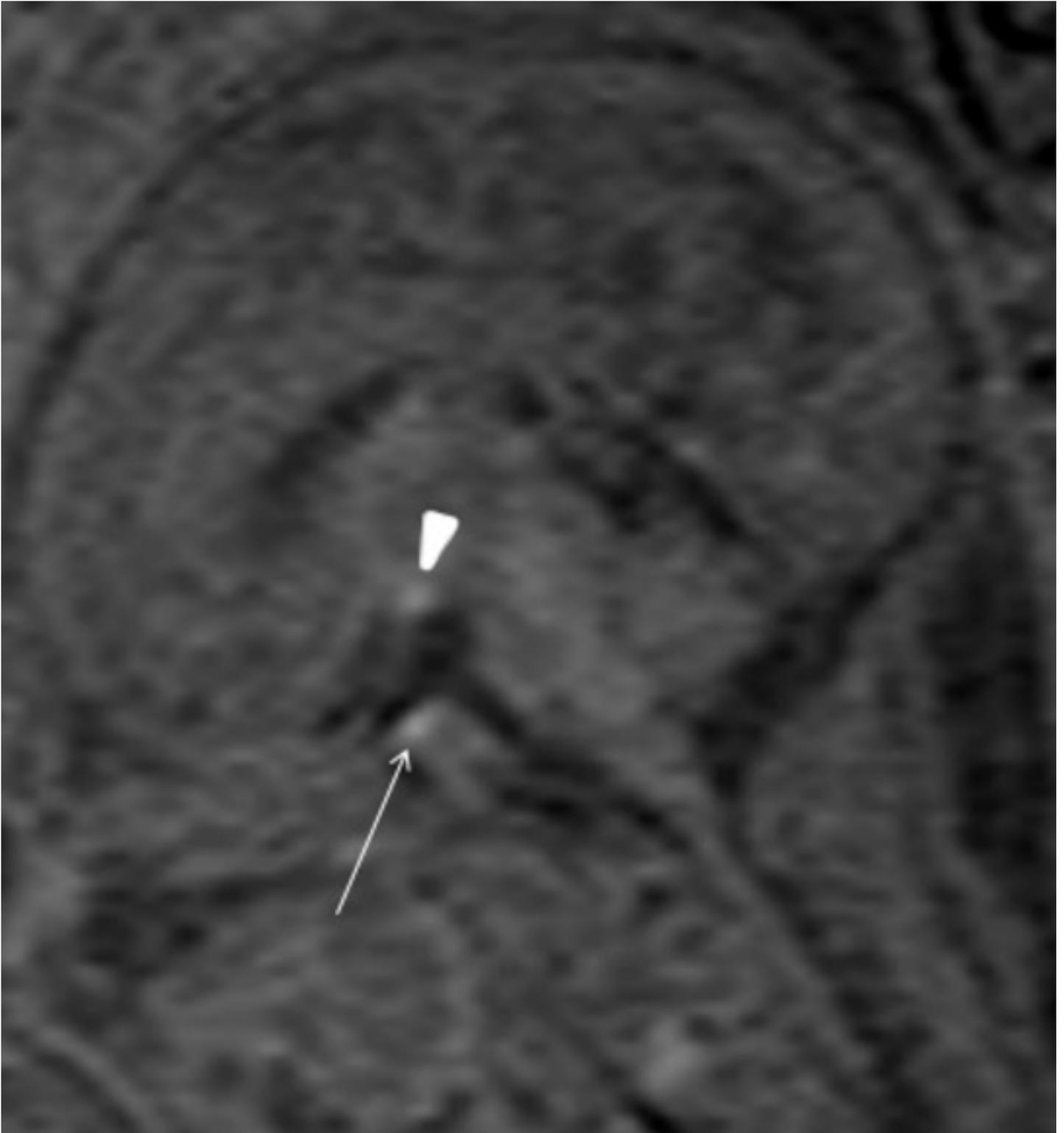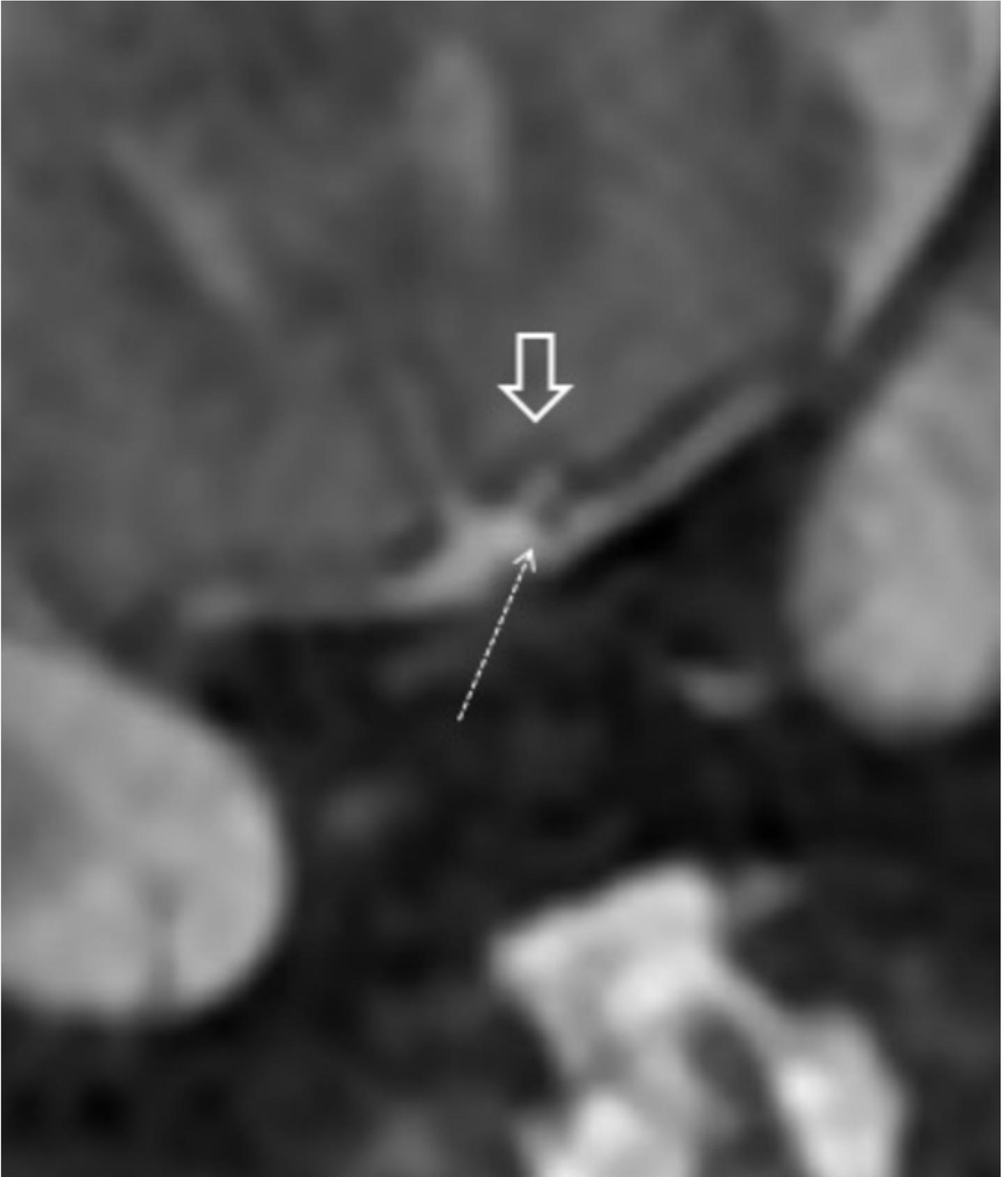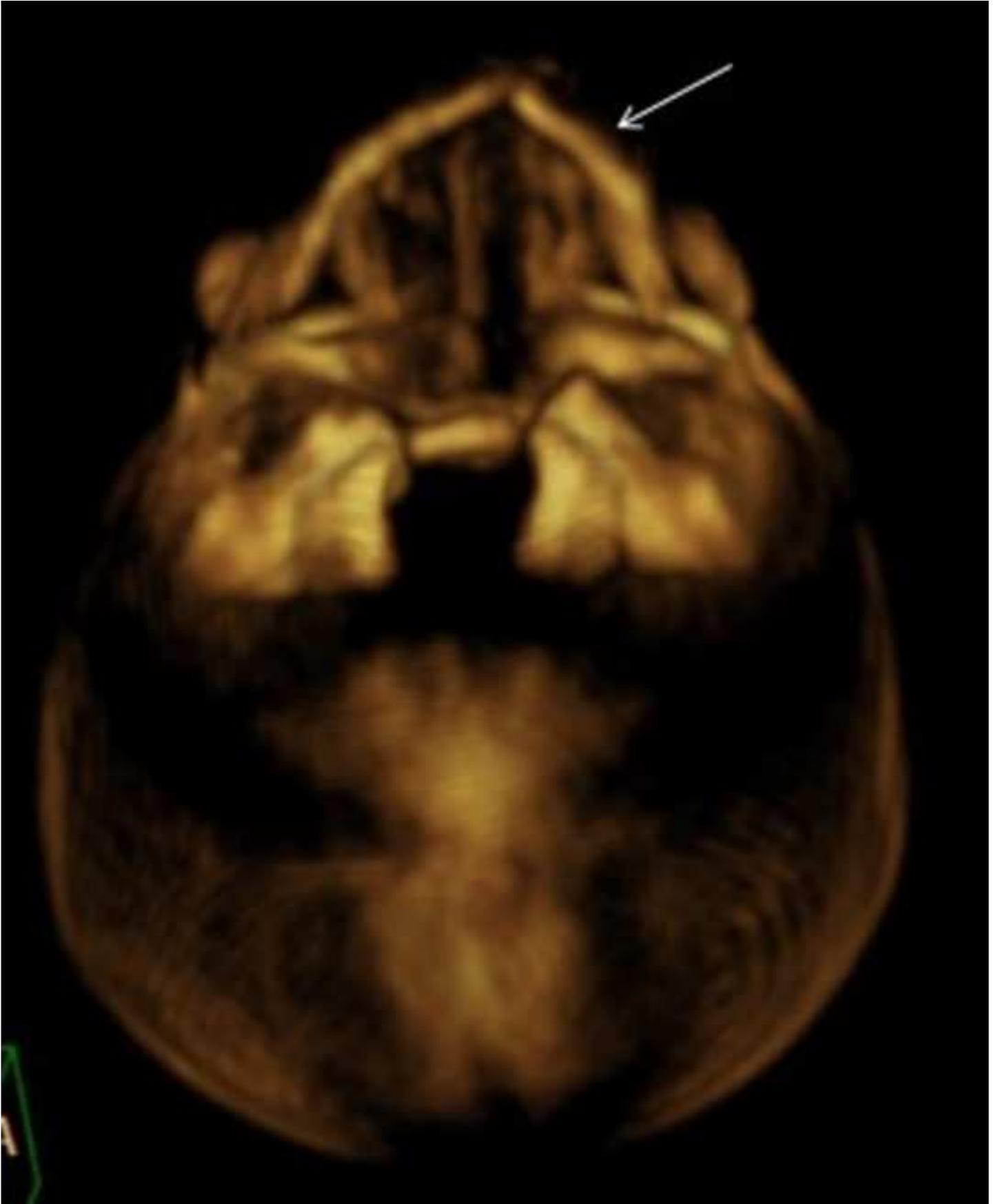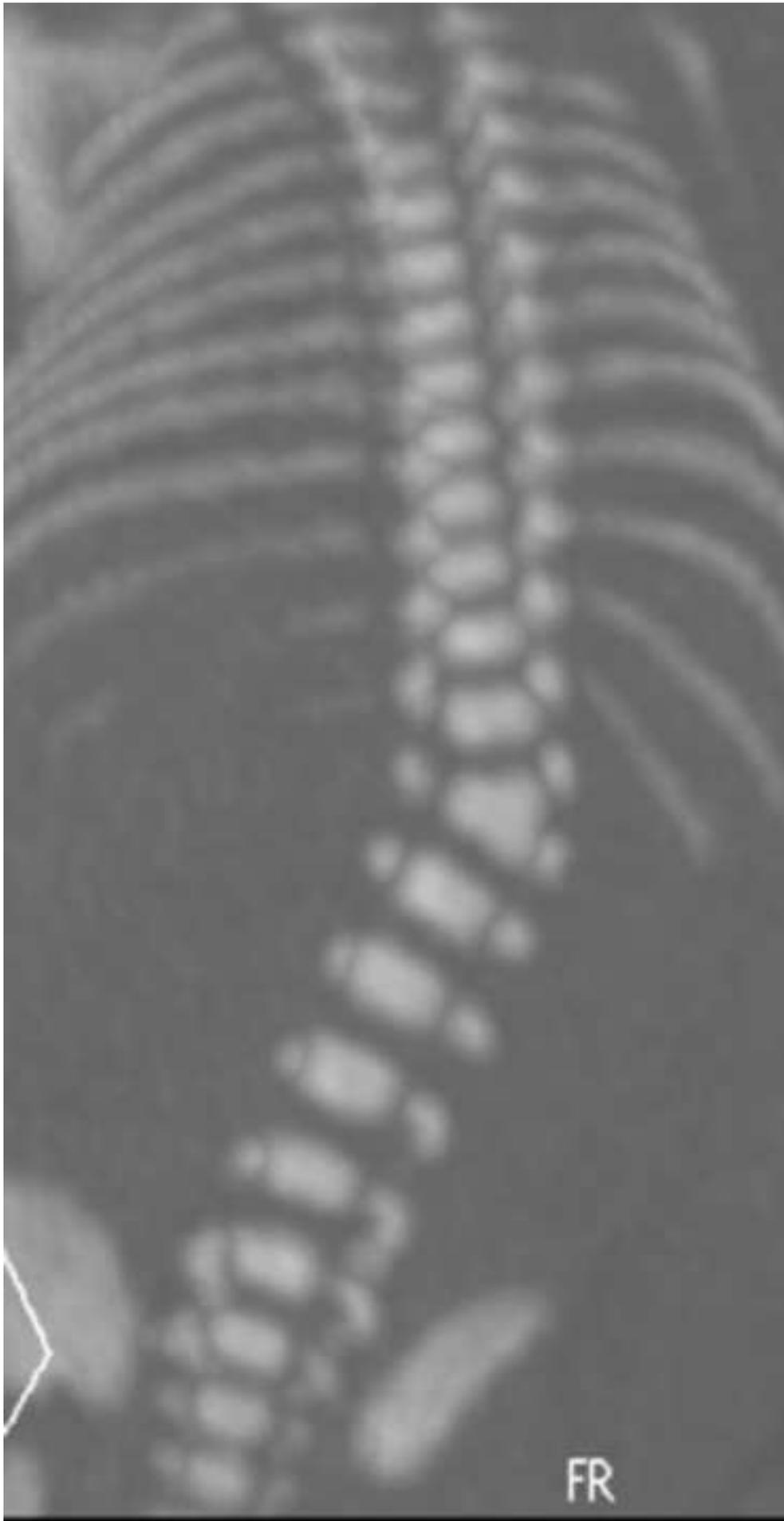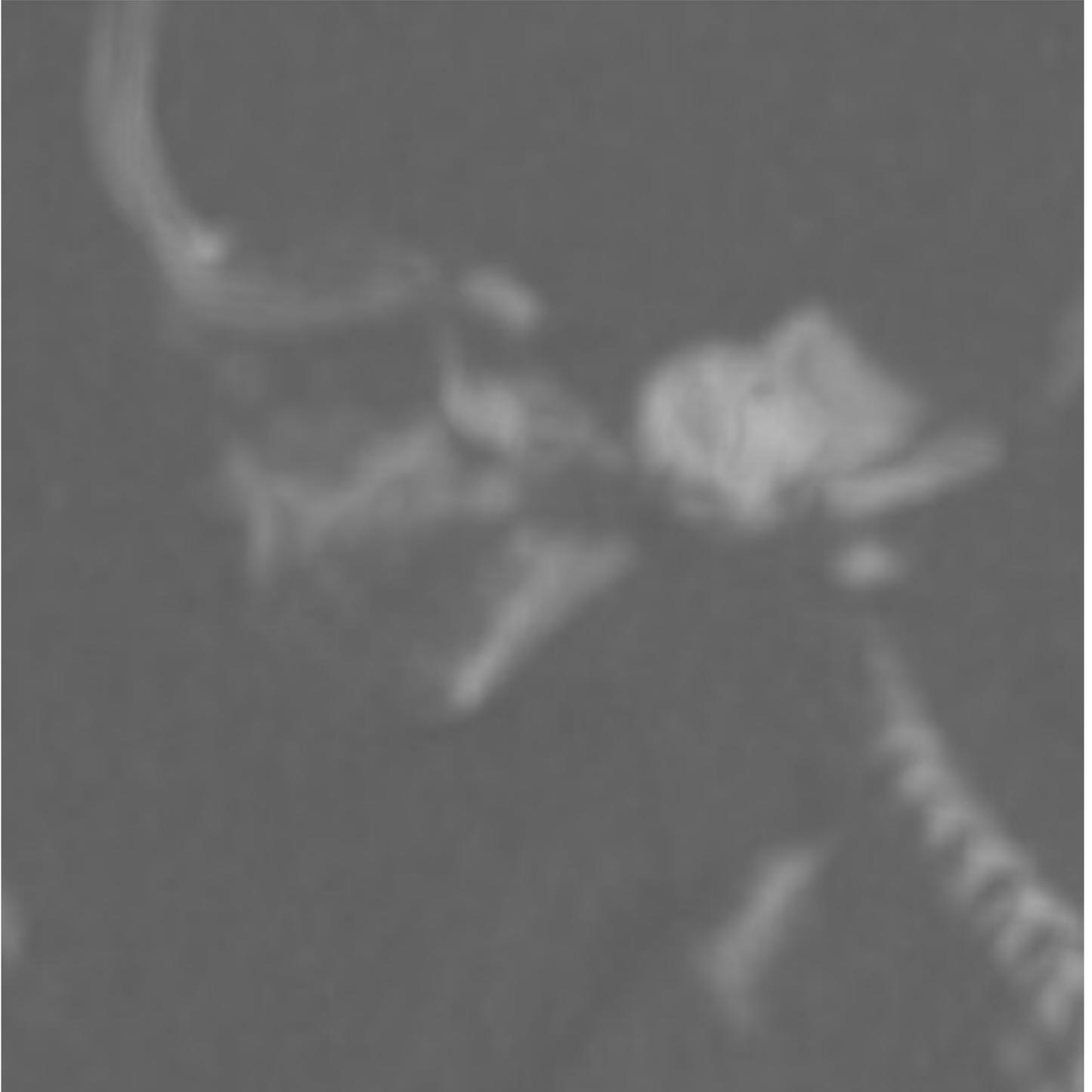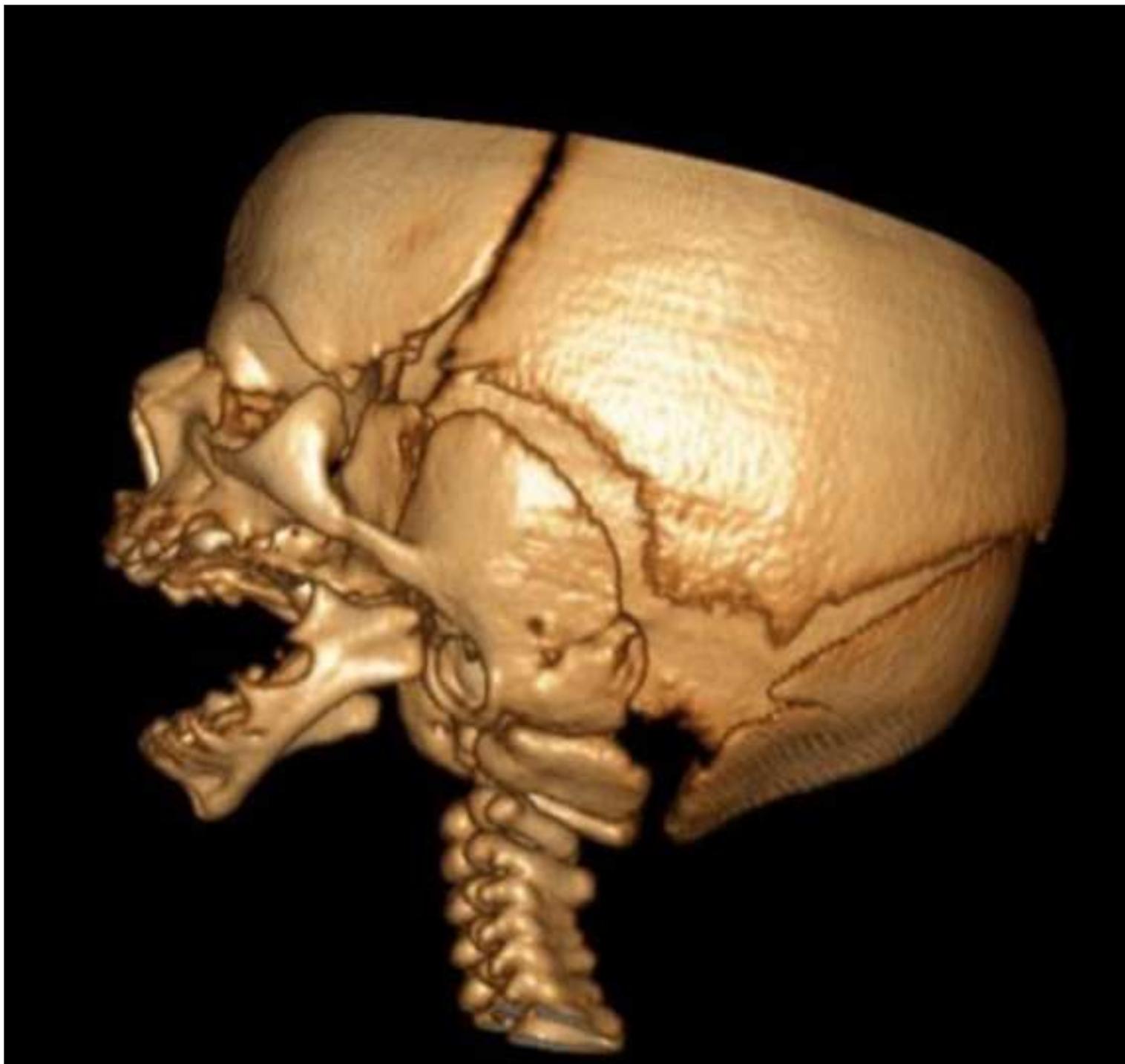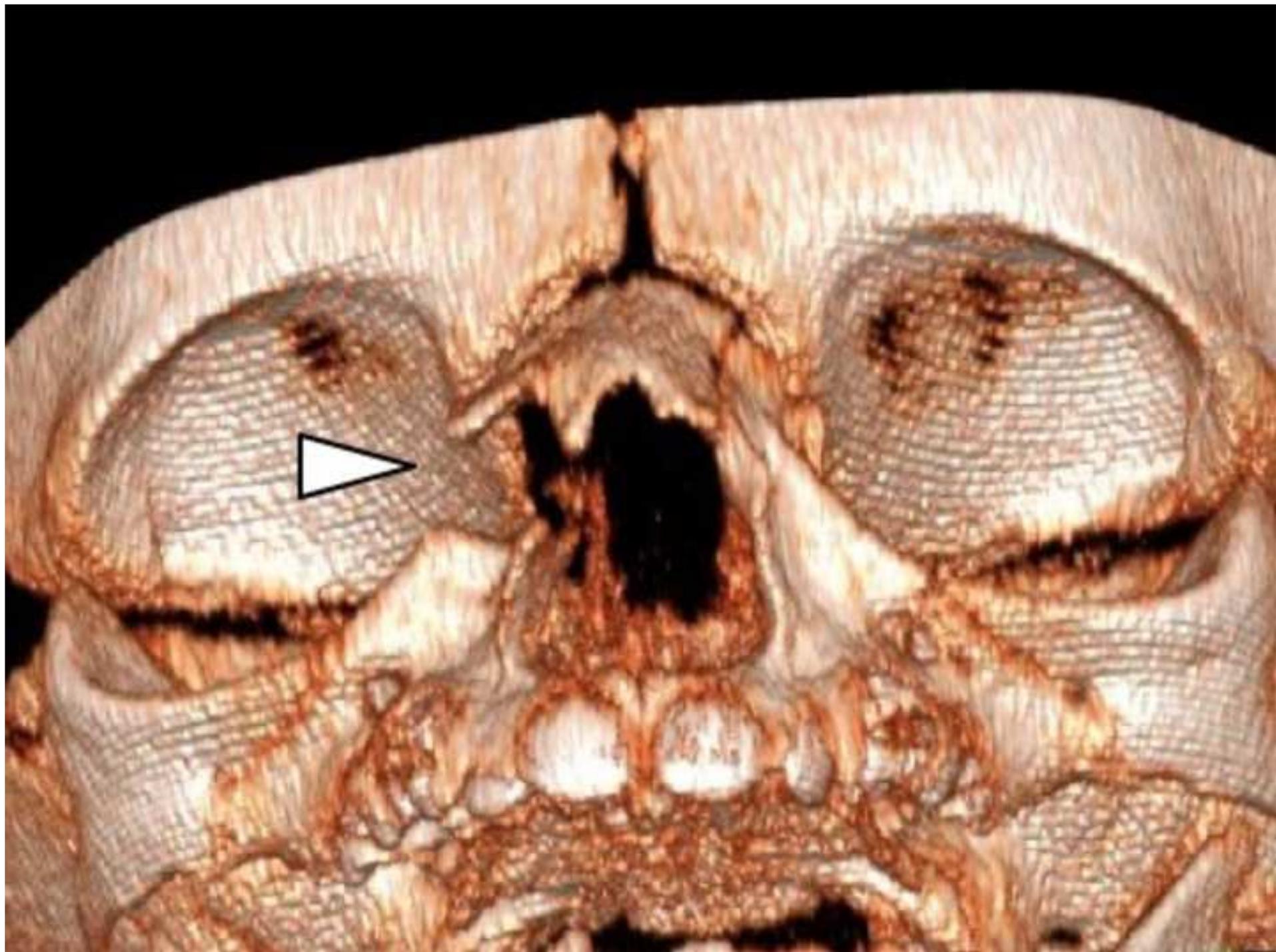
Click here to access/download
Conflict of Interest Form
COI.pdf